Tomáš Blejchař Ph.D.

Best Practice Guide

Numerical simulation of the Selective Catalytic Processes

Best Practice Guide

This project has received funding from the European High-Performance Computing Joint Undertaking (JU) under grant agreement No 951732. The JU receives support from the European Union's Horizon 2020 research and innovation programme and Germany, Bulgaria, Austria, Croatia, Cyprus, the Czech Republic, Denmark, Estonia, Finland, Greece, Hungary, Ireland, Italy, Lithuania, Latvia, Poland, Portugal, Romania, Slovenia, Spain, Sweden, the United Kingdom, France, the Netherlands, Belgium, Luxembourg, Slovakia, Norway, Switzerland, Turkey, the Republic of North Macedonia, Iceland, Montenegro.

Numerical simulation of the Selective Catalytic Processes

Tomáš Blejchař Ph.D.

Best Practice Guide

Contents:

This project has received funding from the European High-Performance Computing Joint Undertaking (JU) under grant agreement No 951732. The JU receives support from the European Union's Horizon 2020 research and innovation programme and Germany, Bulgaria, Austria, Croatia, Cyprus, the Czech Republic, Denmark, Estonia, Finland, Greece, Hungary, Ireland, Italy, Lithuania, Latvia, Poland, Portugal, Romania, Slovenia, Spain, Sweden, the United Kingdom, France, the Netherlands, Belgium, Luxembourg, Slovakia, Norway, Switzerland, Turkey, the Republic of North Macedonia, Iceland, Montenegro.

Nomenclature

A	Pre-exponential factor	$[(\mathrm{mol}\cdot \mathrm{m}^{-3})^{1-\mathrm{n}}/s]$
c_v	Specified heat at constant volume	$[\mathrm{J}/(\mathrm{m}^3\cdot \mathrm{K})]$
c_p	Specified heat at constant pressure	[J/(kg·K)]
$c_{1\varepsilon}$	Empirical constant	[1]
$c_{2\varepsilon}$	Empirical constant	[1]
$c_{3\varepsilon}$	Empirical constant	[1]
C_2	Constant	[1]
C_D	Empirical constant	[1]
C_υ	Constant	[1]
C_μ	Constant	[1]
C_η	Empirical constant	[1]
Da	Damköhler number	[1]
D_i	Diffusion coefficient	$[\mathrm{m}^2/\mathrm{s}]$
E	Energy	[J/kg]
G	Thermic production of turbulent kinetic energy	$[\mathrm{m}^2/\mathrm{s}^3]$
G_b	Production of turbulent kinetic energy due buoyancy	$[\mathrm{kg}/(\mathrm{m}\cdot\mathrm{s}^3)]$
G_k	Production of turbulent kinetic energy due velocity gradient	$[\mathrm{kg}/(\mathrm{m}\cdot\mathrm{s}^3)]$
G_υ	Production of turbulent viscosity	$[\mathrm{kg}/(\mathrm{m}\cdot\mathrm{s}^2)]$
g	Gravity acceleration	$[\mathrm{m}/\mathrm{s}^2]$
h	Enthalpy	[J/kg]

h	Cell height	[m]
I	Spectral radiation intensity	[W/(sr·m)]
K_a	Absorption coefficient	[1/m]
K_s	Scattering coefficient	[1/m]
k	Turbulent kinetic energy	$[\mathrm{m}^2/\mathrm{s}^2]$
K	Reaction rate constant	$\left[(\mathrm{mol}\cdot\mathrm{m}^{-3})^{1-\mathrm{n}}\cdot\mathrm{K}^{\beta}/s\right]$
M	Molar mass	[kg/kmol]
Ma	Mach number	[1]
m	Mass	[kg]
n	Substance amount	[kmol]
n	Reaction order	[1]
P	Mechanical production of turbulent kinetic energy	$[\mathrm{m}^2/\mathrm{s}^3]$
p	Pressure	[Pa]
p_a	Atmospheric pressure	[Pa]
Pr_t	Prandtl turbulent number	[1]
Q	Volume flow	$[\mathrm{m}^3/\mathrm{s}]$
Q_m	Mass flow	[kg/s]
r	Radius vector	[m]
Re	Reynolds number	[1]
R	Universal gas constant	$[\mathrm{J}/(\mathrm{K}\cdot\mathrm{kmol})]$
R_i	Production rate of i^{th} species due chemical reaction	$[\mathrm{kg}/(\mathrm{m}^3\cdot\mathrm{s})]$
r	Gas constant	[J/(kg·K)]

S	Surface, Area	$[m^2]$
S_i	Production rate of distributed species	$[kg/(m^3 \cdot s)]$
Sc_t	Schmidt turbulent number	[1]
S_k	Users defined source term of turbulent kinetic energy	$[kg/(m \cdot s^3)]$
S_ε	Users defined source term of dissipation rate	$[kg/(m \cdot s^4)]$
S_υ	Users defined source term of viscosity	$[kg/(m \cdot s^2)]$
T	Thermodynamic temperature	[K]
T^*	Dimensionless temperature	[1]
t	Relative temperature	[°C]
t	Time	[s]
u	Velocity	$[m/s]$
u_i	i^{th} component of velocity	$[m/s]$
$\overline{u_i}$	i^{th} component of mean velocity	$[m/s]$
x_i	Coordinates $[x_1, x_2, x_3]$ or [x, y, z]	[m]
X_i	Molar fraction of i^{th} component of mixture	[1]
Y_i	Mass fraction of i^{th} component of mixture	[1]
Y_M	Fluctuation dilatation source term	$[kg/(m \cdot s^3)]$

Greek letters:

α	Volume fraction	[1]
β	Temperature exponent	[1]
β	Stoichiometric ratio	[1]
δ_{i3}	Kronecker delta	[1]

ε	Dissipation rate	$[m^2/s^3]$
ε	Spectral emissivity	[1]
γ	Heat capacity ratio, Adiabatic index	[1]
λ	Thermal conductivity	$[W/(m \cdot K)]$
η	Dynamic viscosity	$[Pa \cdot s]$
η_{eff}	Effective viscosity	$[Pa \cdot s]$
η_t	Turbulent viscosity	$[Pa \cdot s]$
υ	Viscosity	$[m^2/s]$
υ_t	Turbulent viscosity	$[m^2/s]$
ρ	Density	$[kg/m^3]$
τ	Shear stress	[Pa]
τ_{jl}	Shear stress tensor	[Pa]
σ_k	Empirical constant	[1]
σ_ε	Empirical constant	[1]

List of Abbreviations:

AIG	Ammonia injection grid
CFD	Computation Fluid Dynamics
LES	Large Eddy Simulation
RANS	Reynolds Average Navier-Stokes
RNG	Re-Normalization Group
SCR	Selective Catalytic Reduction
SNCR	Selective Non-Catalytic Reduction

1 Introduction

The role of nitrogen oxides in the formation of photochemical smog has been discussed since 1952. These chemical species are considered potential air pollutants. NO_x, which includes nitric oxide NO and the nitrogen dioxides NO_2, contributes to acid rain, reduced visibility, and fine particle. Photochemical air smog is a complex mixture of gaseous pollutants. The contribution of NO_x is represented by the following chemical reactions:

$$\begin{aligned} &NO_2 + hv \rightarrow NO + O\cdot \\ &O\cdot + O_2 + M \rightarrow O_3 + M \\ &O_3 + NO \rightarrow O_2 + NO_2 \end{aligned} \qquad (1.1)$$

Dynamic equilibrium of previous chemical reactions established in the atmosphere is given by summary reaction:

$$NO_2 + O_2 \overset{hv}{\rightarrow} NO + O_3 \qquad (1.2)$$

However, the reactions of atomic oxygen $O\cdot$ with various hydrocarbons, olefins, benzene, etc., emitted in the exhaust gas of mobile combustion units or the flue gas of stationary combustion units, also form free radicals. Other reactions may form unpleasant organic compounds such as aldehydes, formaldehyde, ketones, or nitrogen-containing compounds. These chemical compounds are primarily compounds in the photochemical smog.

The sulphuric acid H_2SO_4 and the nitric acid HNO_3 are the main component of the atmosphere able to form acid rain. The chemical reactions that mainly convert nitric dioxide NO_2 to nitric acid HNO_3 and sulphur dioxide SO_2 to sulphuric acid H_2SO_4 include the $OH\cdot$ radical.

$$\begin{aligned} &NO_2 + OH\cdot \rightarrow HNO_3 \\ &SO_2 + OH\cdot \rightarrow \cdots \rightarrow H_2SO_4 \text{ (multi-steps)} \end{aligned} \qquad (1.3)$$

The concentration of OH^- radical depends indirectly on the NO_x level and hydrocarbons, and the sunlight intensity. The concentration of nitric acid HNO_3 is directly dependent on NO_x emission. H_2SO_4 and HNO_3 production is influenced in a complex and non-linear way by the concentration of NO_x and hydrocarbons C_xH_y through their effect on $OH\cdot$ radical concentration. The impact of acid rain can be traced to the acidification of water (lakes, rivers, surface water), damaging the ecosystem.

Nitrogen oxides NO_x are also involved in the production of fine particles. Fine particles (diameter is less than 2.5 μm that exist as liquid or solid) are in the atmosphere under normal conditions. The main reason for the control of particle organic matter is their long-term health hazard. The issue with organic compounds (polycyclic aromatic hydrocarbons etc.) is potentially carcinogenic and mutagenic. The particular matter is responsible for visibility reduction too.

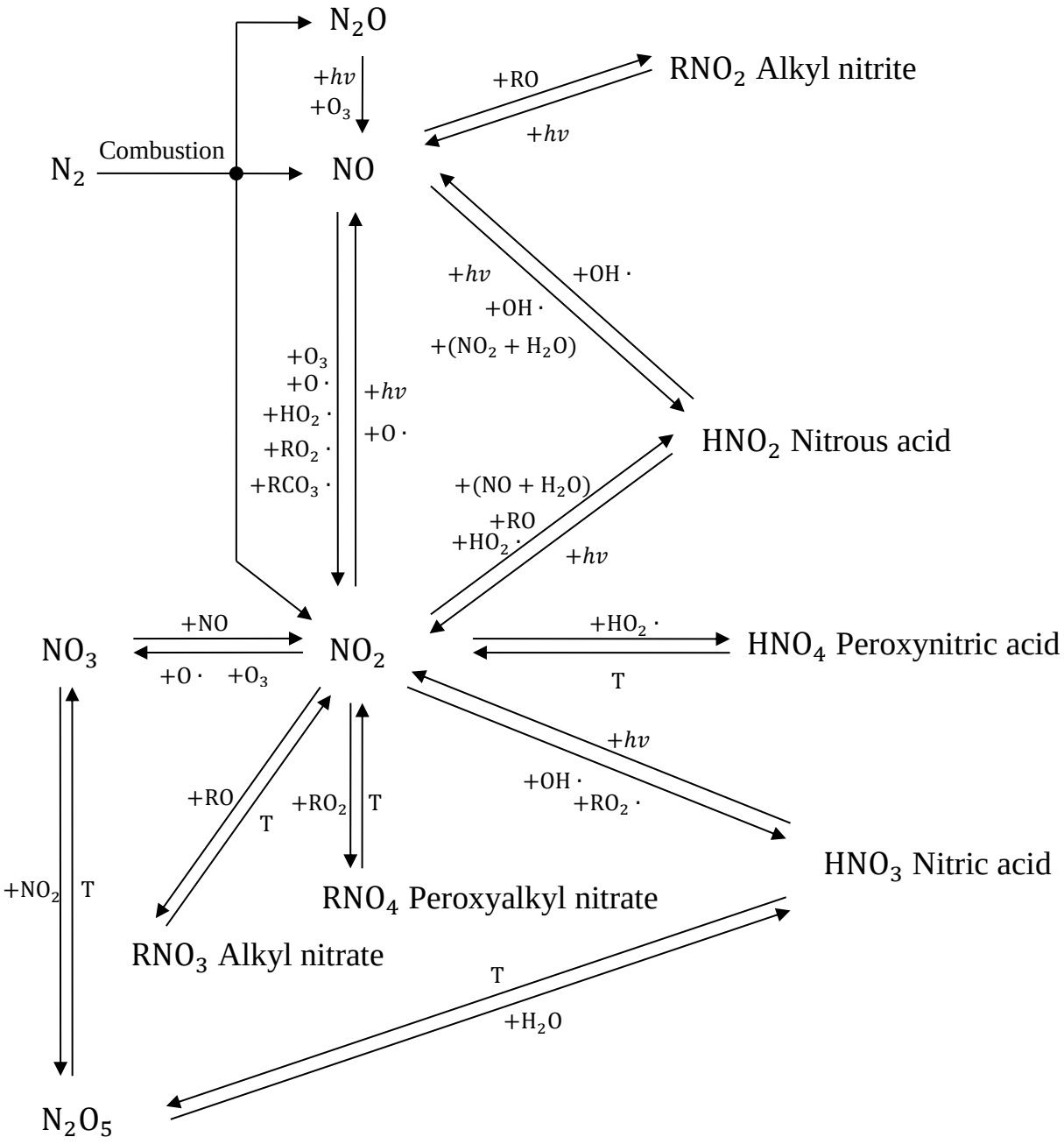

Fig. 1.1 Chemical transformation of the nitrous oxides NO_x in the atmosphere

1.1 Formation of Nitrogen Oxides

The NO_x is mainly composed of nitric oxide NO (c. 90–95%) and nitrogen dioxide NO_2 (c. 5–10%). As we say, NO_x reacts to form smog and acid rain. Nitrous oxide N_2O is not a component of NO_x, but it is a greenhouse gas and is also produced by the combustion process.

The nitrogen oxides NO_x produced from the combustion process are generated in three different ways.

1) Thermal nitrogen oxides NO_x
2) Prompt nitrogen oxides NO_x
3) Fuel nitrogen oxides NO_x

1.1.1 Thermal NO_x

Production of thermal NO_x dominantly depends on the temperature of the combustion process. The thermal NO_x is formed from the free radical $O\cdot$ and $N\cdot$, which are occurred at higher temperatures. The mechanism of thermal NO_x production is represented by the following chemical reactions, which Zeldovich proposed:

$$N\cdot + O_2 \leftrightarrow NO + O\cdot \quad (1.4)$$

$$N_2 + O\cdot \leftrightarrow NO + N\cdot \quad (1.5)$$

$$N\cdot + OH\cdot \leftrightarrow NO + H\cdot \quad (1.6)$$

The kinetics of previous chemical reactions depends not only on temperature but also on the local stoichiometry and residence time. The production of thermal NO_x becomes essential only for the temperature of the combustion process above 1500°C. The rate of NO_x production doubles up for increasing flame temperature by about 40°C. The NO_x production rate is also equal to the partial pressure of oxygen O_2. However, the increasing concentration of oxygen O_2 in the combustion zone reduces the flame temperature, which is the opposite of the partial pressure of oxygen. The oxygen radical $O\cdot$ concentration is equal to the dissociation of molecular oxygen O_2at a higher temperature.

$$O_2 \leftrightarrow 2\,O\cdot \quad (1.7)$$

1.1.2 Prompt NO_x

Prompt NO_x formation is related to rapid and complex chemical reactions, which occur near the flame zone. There is a reaction between hydrocarbon radicals $CH_y\cdot$ and nitrogen N_2, and the product of this reaction may be oxidised to NO under fuel-rich conditions.

$$CH\cdot + N_2 + O_2 \rightarrow HCO + NO + N\cdot \quad (1.8)$$

The complete mechanism of production of prompt NO_x is very complicated, and it must be simplified.

1.1.3 Fuel NO_x

Fuels such as coal fuel oil contain organically bound nitrogen N_2. The organic compounds in fuel react with combustion air, and the product of this reaction is fuel NO_x. The process of fuel NO_x formation is still not precisely understood. Still, it is known that the production of fuel NO_x is more sensitive to local combustion stoichiometry (fuel/air ratio) than to combustion temperature, and it is commonly represented using hydrocyanic acid HCN.

$$HCN + O_2 \rightarrow HCO + NO \quad (1.9)$$

$$4\,HCO + 3\,O_2 \rightarrow 4\,CO_2 + 2\,H_2O \quad (1.10)$$

1.2 Methods of Nitrogen Oxides Reduction

The most significant percentage of NO_x (c 70%) is a product of human activities despite NO_x produced by natural processes. Controlling NO_x emission is currently a problem solution under the local environmental protection agency (Ministry of the Environment). Two different strategies for the reduction of NO_x are known. The methods are known as combustion and post-combustion method. They are also known as primary and secondary measures.

1.2.1 Combustion Method

Several methods can control the emission of NOx. Some of these techniques are based on a modification of the combustion process, such as flue gas recirculation (FGR), reburning, staged air addition (OFA-overfire air), and steam of water injection (SI)/(WI). Every previously listed method modifies local stoichiometry and/or combustion temperature, whereby the reduction of NO_x emission is achieved. An alternative approach is based on the installation of Low-Emission Burners (LNB) in the combustion chamber.

1.2.2 Post-Combustion Method

Post-combustion methods can be divided into three different types. The names of these methods are Selective Catalytic Reduction (SCR), Selective Non-Catalytic Reduction (SNCR) and Non-Selective Catalytic Reduction (NSCR).

The mobile sources of NO_x generally use highly refined fuel such a gasoline or diesel oil. That means the fuel NO_x is not almost formed. Primary sources of NO_x are prompt and thermal. Modification of the combustion process is not recommended because other pollutant emissions influence it. Modern automotive engines usually drive the combustion process utilising exhaust gas recirculation (EGR-valve), limiting oxygen O_2 during fuel combustion. Whereas the refined fuel is used, the combustion products do not contain species (like ash); this makes it reasonable to use Non-Selective Catalytic Reduction (standard catalyst) and Selective Catalytic Reduction (Ad-blue technology), which is realised in automotive emission control systems.

Stationary sources of NO_x produces the flue gas, which concentration of oxygen O_2 is more significant than nitrous oxides NO_x. That is why selective NO_x control (SNCR/SCR) need to be used. The chemical compound selective deoxidises the NO_x with or without a catalyser (SCR or

SNCR), and the product of the deoxidise process is the molecular form of nitrogen N_2 and water H_2O.

SCR methods post-combustion strategies of NO_x reduction is based on deoxidise process on the surface of the catalyst bed. The bed is located downstream of the boiler. However, typically power plant produces flue gas containing large amounts of catalytic poison (e.g., sulphur dioxides), which relative rapidly foul and plug the catalytic bed. It means that the efficiency of the SCR process falls, and pressure drop is becoming high. Among others, very high capital costs and considerable space are required.

SNCR Post-combustion strategies of NO_x reduction is based on injection of chemical compound downstream to main combustion region. Three different commercial processes are used in the present: Thermal DeNO$_x$, RAPRENO$_x$, and NO$_x$OUT. These methods involve the addition of ammonia NH_3, cyanuric acid $(HCNO)_3$ and urea $CO(NH_2)_2$. The main advantage of this process is the low capital cost. However, the reduction of NO_x is only 50–65% in a typical boiler, and the SNCR processes achieve reasonable NO_x reduction only in a narrow range of temperature (extremity 750–1050°C, optimum 950°C).

2 Background of SCR and SNCR Technology

Both techniques SCR and SNCR, are based on the chemical reaction of ammonia radical $NH_2 \cdot$ with NO_x.

$$NH_2 \cdot + NO \rightarrow N_2 + H_2O \tag{2.1}$$

The chemical kinetics of SNCR or SCR is relatively complicated, and all processes are not yet fully understood. The summarised reduction path diagram of NO_x is in Fig. 2.1. The diagram includes all three commonly used addition. In the following chapters, the chemical kinetics of SCR and SNCR are presented.

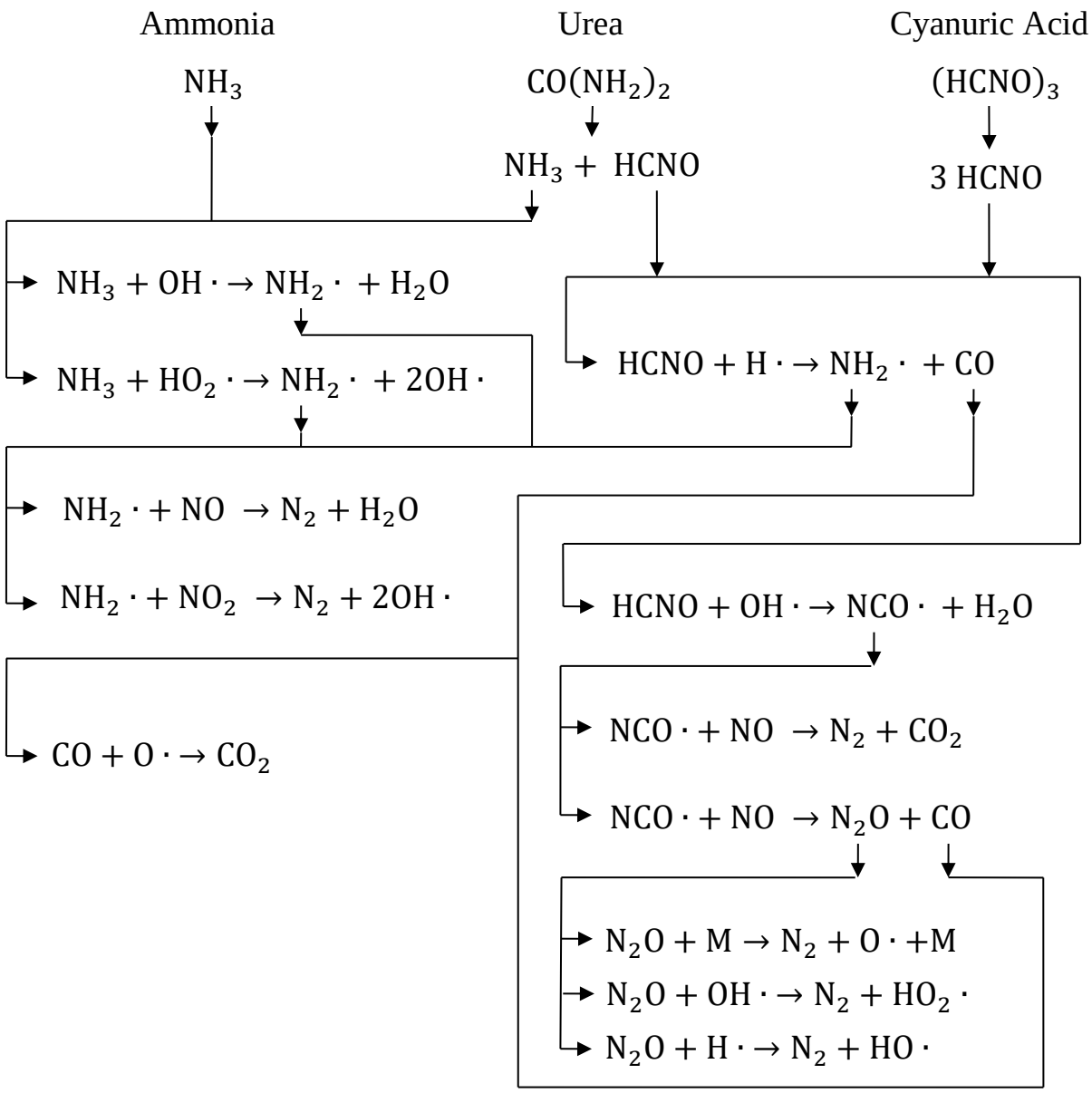

Fig. 2.1 Reaction path diagram for the NO_x reduction [1]

2.1 SCR Method

The SCR method was initially invented in the USA in 1959. Development of this method includes laboratory experiments, which led to catalyst material estimation, the real-life catalyst test and optimising process. The first commercial realisation was in Japan in 1978. The SCR technology has been commercialised in Germany since 1985 [2].

Catalytic reduction of NO_x is realised on the active surface of the catalyser, which is usually designed as a ceramic monolith with dashed active material. Reduction usually occurs in the range of temperature 320–400°C. The efficiency of the reduction process is generally 80–90%.

2.1.1 Basic Chemistry of SCR

In selective catalytic reduction, the NO_x in flue gas is selectively reduced to nitrogen N_2 and water vapour H_2O by reaction with ammonia NH_3 in the presence of a catalyst. The SCR process can be described by the following chemical reactions [3]:

$$4\,NO + 4\,NH_3 + O_2 \xrightarrow{\text{catalyst}} 4\,N_2 + 6\,H_2O \tag{2.2}$$

$$2\,NO + 4\,NH_3 + O_2 \xrightarrow{\text{catalyst}} 3\,N_2 + 6\,H_2O \tag{2.3}$$

$$6\,NO + 4\,NH_3 \xrightarrow{\text{catalyst}} 5\,N_2 + 6\,H_2O \tag{2.4}$$

$$6\,NO + 8\,NH_3 \xrightarrow{\text{catalyst}} 7\,N_2 + 12\,H_2O \tag{2.5}$$

$$2\,NO_2 + 4\,NH_3 + O_2 \xrightarrow{\text{catalyst}} 3\,N_2 + 6\,H_2O \tag{2.6}$$

$$NO + NO_2 + 2\,NH_3 \xrightarrow{\text{catalyst}} 2\,N_2 + 3\,H_2O \tag{2.7}$$

The catalyst lowers the activation energy of the chemical reactions. With most catalysts, the operating temperature of the SCR process is limited to 400°C. This limit prevents catalyst sintering and consequent deactivation. The lower temperature is limited to about 260–300°C. The lower operating temperature depends on the sulphur dioxide SO_2 and/or sulphur trioxide SO_3 concentration in the flue gas. If the operating temperature is too low, then the sulphur trioxide SO_3 in flue gas can evoke ammonium sulphate $(NH_4)_2SO_4$ and ammonium bisulphate deposition $(NH_4)HSO_4$ on the active surface of the catalyst bed. This process typically occurs at a temperature between 90–170°C. The deposit is very hard and deactivates the catalyst. Ammonium sulphate is also formed as a fine powdery substance at a temperature of 260°C, but an electrostatic precipitator can remove this substance. The production of ammonium sulphate and bisulphate can be described by the following chemical reactions [1]:

$$2\,SO_2 + O_2 \rightarrow SO_3 \tag{2.8}$$

$$SO_3 + 2\,NH_3 + H_2O \rightarrow (NH_4)_2SO_4 \tag{2.9}$$

$$SO_3 + NH_3 + H_2O \rightarrow (NH_4)HSO_4 \tag{2.10}$$

The chemical reaction involving the oxygen O_2 comprises the dominant path for NO_x required concentration of oxygen is 1% by volume as a practical minimum. The SCR process usually has a molar ratio of injected ammonia to reduced nitrous oxides $NH_3/NO_x \cong 1$ as a practical value.

2.1.2 Ammonia slip

Ammonia slip represents a concentration of residual reagent, which is in flue gas downstream of the main reaction zone. Ammonia slip levels of about 20 mg/m_N^{-3} or less do not present a significant environmental concern. Still, it may lead to the formation of ammonia salts, which could cause secondary problems downstream the main combustion zone as deposits on heat exchangers (air pre-heater, rotating plate regenerative air pre-heater, etc.) of ammonium sulphate and/or bisulphate and a visible detached plume of ammonium chloride due to next reactions [1]:.

$$SO_3 + 2\,NH_3 + H_2O \rightarrow (NH_4)_2SO_4 \quad (2.11)$$

$$SO_3 + NH_3 + H_2O \rightarrow (NH_4)HSO_4 \quad (2.12)$$

$$NH_3 + HCl \rightarrow NH_4Cl \quad (2.13)$$

Ammonium sulphate and/or bisulphate and ammonium chloride are fine powder substances. These products can evoke deposition of these substances on the walls of the flue gas patch. This deposit reduces the efficiency of heat exchangers (air pre-heater, rotating plate regenerative air pre-heater, etc.) due to the low thermal conductivity of the deposit. Another problem is the high-pressure drop of heat exchangers with the deposit of ammonia salts.

In many cases, the fly ash is used as plaster material in underground mining or used as a power plant product for which the adding of water is necessary. Water released the ammonia, and the products smell. In these areas, the smell of ammonia is not acceptable; therefore, the ammonia slip should be controlled at a minimum. An optimum value of ammonia slip is below 5 mg/m_N^{-3}, which was evaluated based on the long-term optimisation of SCR technology.

2.1.3 SCR Application for Boiler

The catalyst reactor located in the flue gas path can be realised in three ways, and that is why the SCR system is classified into one of the categories:

Hot-side, high-dust system – The catalyst rector is located downstream of the economiser (ECO) and upstream of the air pre-heater and emission control equipment. This is the most used configuration of SCR if the required reaction temperature range is available, and no auxiliary heat source is required. The main disadvantage of this configuration is loaded with heavy dust flue gas. The matter of catalytic bed is limited to minimal oxidation of SO_2 to SO_3 eq. (2.8) to prevent ammonium sulphate and bisulphate production. The presence of ash in flue gas also increases the volume of the catalytic bed. The presence of ash in flue gas assists the process of removing (abrasive effect of particles) sulphates hard deposit of from catalyst. However, the particles also cause the erosion of the catalytic bed and deactivation (chemical poisoning). Required space for SCR catalyst reactor is a consideration with this configuration too.

Hot-side, low-dust system – The catalyst reactor is located downstream of the hot electrostatic precipitator and upstream of the air pre-heater and desulphurisation technology. The main advantage of this configuration is the absence of fly ash in the flue gas. It minimises erosion of the catalytic bed and deactivation. The flying ash removed upstream of the SCR catalyst is not also

contaminated by ammonia because ammonia contamination fly ash can potentially cause the deactivation (poisoning) of the catalyst. A disadvantage of this configuration is the hot-side electrostatic precipitator and predisposition of the catalytic bed to aggradation with fine ash particle and ammonium sulphate and bisulphate.

Cold-side, low-dust system – The catalyst reactor is located at the end of the flue gas path. It means the catalyst is located downstream of an air pre-heater, electrostatic precipitator, and desulphurisation technology. The name of the configuration is also the tail-end system. Since the fly ash and sulphur oxides, SO_x is removed upstream, the catalyst bed required volume is least. However, flue gas temperature is generally low, and this SCR configuration requires an auxiliary heat source to reheat flue gas. The disadvantage is the relatively high cost associated with the auxiliary heat source. The cost of an auxiliary heat source is usually greater than cost savings resulting from minimised catalytic bed volume. This configuration is applied only on boilers where the previous configuration cannot be applied due to space limitations. This configuration is also applied to waste incineration plants, where it is prudent to remove the acidic gases.

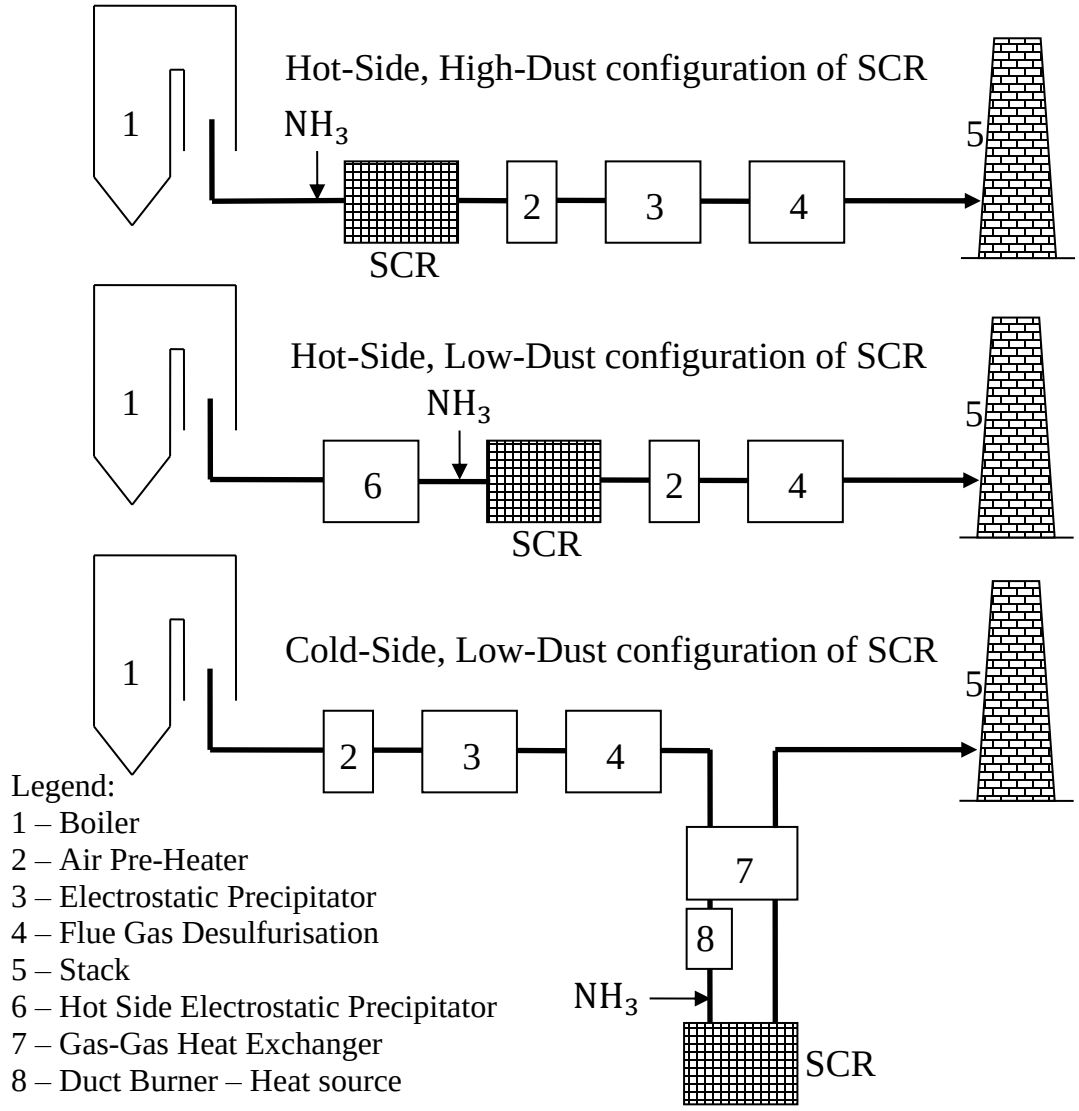

Fig. 2.2 Basic SCR configurations [2]

SCR technology always includes three main components without reference to the basic configuration.

1) Ammonia, ammonia water urea solution storage tank.
2) Injection nozzles so-called AIG (Ammonia Injection Grid).
3) SCR reactor and by-pass duct.

The SCR reactor is usually composed of metal oxides such as titanium TiO_2 or vanadium V_2O_5. These oxides are donated by other metal oxides such as molybdenum Mo, wolfram W, seldom iron Fe, cobalt Co, copper Cu, magnesium Mg, zinc Zn, aluminium Al, etc. Catalyst can also be composed of platinum Pt. The disadvantage of this catalyst is the relatively high cost. This catalyst can operate within a temperature window of 210–280°C with an optimum operating temperature

of about 250°C. Recently, high-temperature zeolite catalysts have been introduced. The zeolite catalysts are stable over a wider temperature range than the metal oxides catalysts. Other materials used as porous ceramic matrices are aluminium oxide Al_2O_3, iron trioxide Fe_2O_3, silicon dioxide SiO_2. The main advantages of this catalyst are simply manufacturing (mould pressing) and non-problematic used catalyst disposal because the catalyst does not contain heavy metals and is not classified as non-hazardous waste. This catalyst can be operative within a temperature window of 220–580°C.

There are several requirements in the design of an SCR reactor. The steel support construction is designed as a supporting structure that includes platforms for operation and maintenance of the catalyst units or blocks see Fig. 2.3. The structure must also compensate for the three-dimensional thermal expansion of the catalyst and facilitate catalyst installation, removal, and replacement of the catalyst.

The SCR technology usually includes a by-pass, which is used in the start-up and shutdown of the boiler. The by-pass protects the catalyst when the temperature of flue gas is below the dew point.

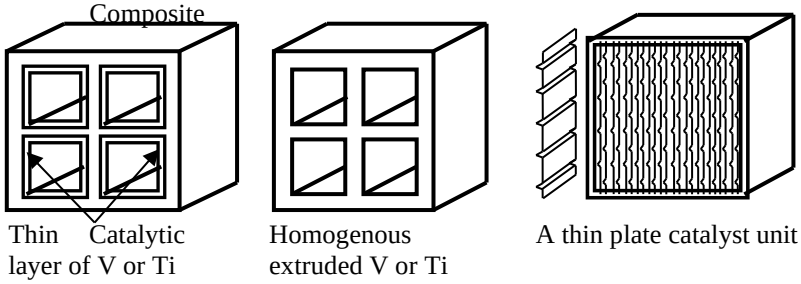

Fig. 2.3 Basic types of SCR catalyst unit (block) [2]

3 Description of SCR Process

The SCR technology usually includes same main parts as SNCR technology. This technology includes injectors or injection grids, and only the catalyst reactor is an additional part compared to SNCR. The SCR technology uses anhydrous and aqueous ammonia as a reagent, which means storing and handling a reagent must be designed for stringent safety requirements. The ordinary specification of an SCR system requires specific design information. The information includes:

1) Initial NO_x concentration in flue gas, flue gas flow.
2) Required reduction of NO_x.
3) Ammonia slip.
4) Excess oxygen concentration.
5) Sulphur is included with fuel and SO_2.and SO_3.concentration in the flue gas.
6) Type of an SCR – Hot-side high-dust, Hot-side low-dust, Colt-side high-dust and location of catalyst.
7) Ash quality and characteristics.
8) Type of fuel.
9) Catalyst life requirements.

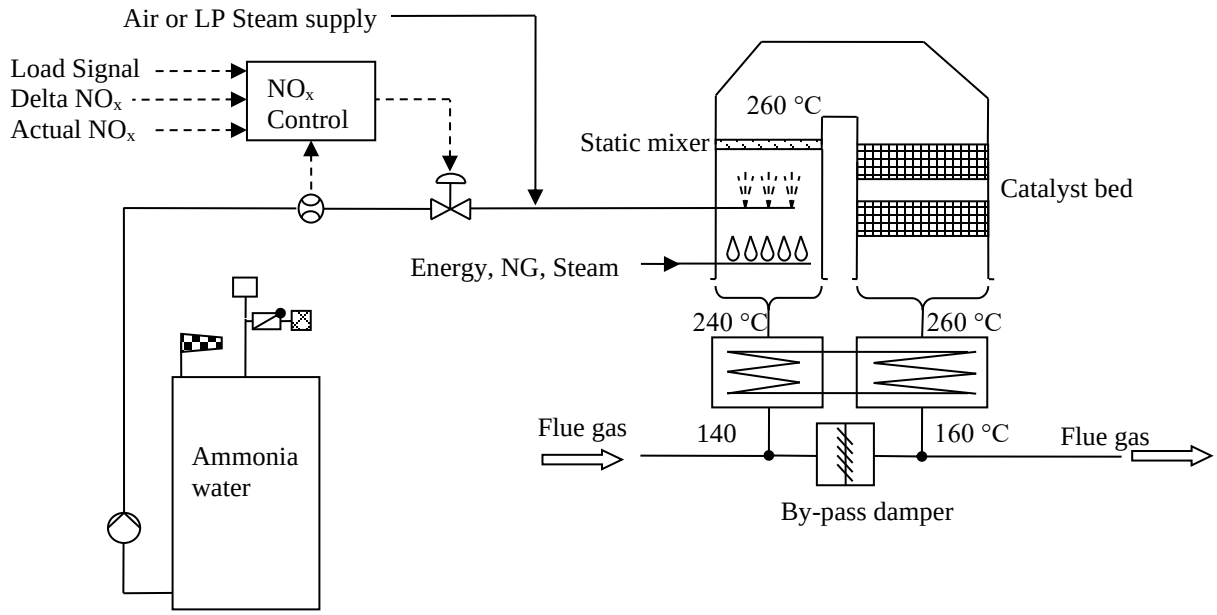

Fig. 3.1 Flow diagram of SCR technology, tail-end system [1]

The mass flow of the required reagent is usually controlled based on the NO_x concentration at the inlet of the SCR. Measurement of the NO_x concentration at the SCR inlet is combined with the flue gas flow yields the NO_x flow signal. The control module multiplies this signal by the set molar ratio β to obtain the regent flow demand signal. The reagent demand signal is compared with the actual reagent flow, and the flow is adjusted to meet the demand. The ammonia slip is

usually measured downstream of the SCR reactor and recorded as the NO_x concentration downstream of the SCR reactor. Reagent flow is shut off by a low-temperature switch when the operating flue gas temperature drops below the minimum recommended value. This control must be applied to prevent the deactivation o the catalyst from ammonium sulphate and/or bisulphate deposition.

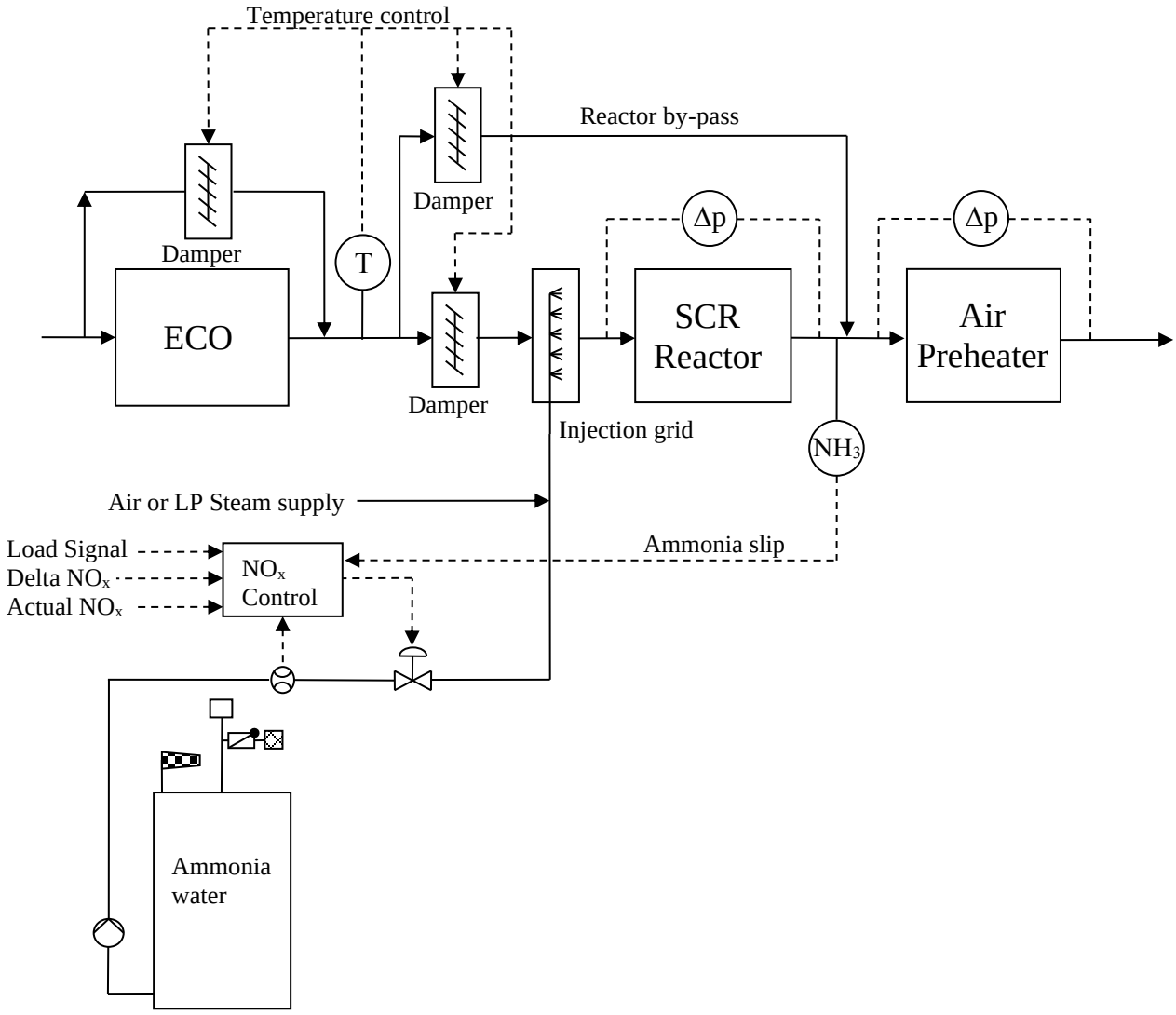

Fig. 3.2 Flow diagram of SCR technology, hot side – high dust system [1]

The SCR technology must include the reactor by-pass. This by-pass protects the SCR reactor during start and shutdown when the flue gas temperature can be below the dew point. The SCR technology sometimes includes the economiser by-pass. An economiser by-pass is used to maintain the flue gas temperature above the SRC reactor recommended minimum.

The SCR method can be installed in front of the HRSG boiler, usually installed downstream of the combustion turbine. The cross-section of the HRSG boiler is relatively large, and the turbine usually uses natural gas as a fuel, so the concentration of SO_2 is irrelevant. That is why this technology does not include a reactor by-pass, and temperature control is not necessary to install.

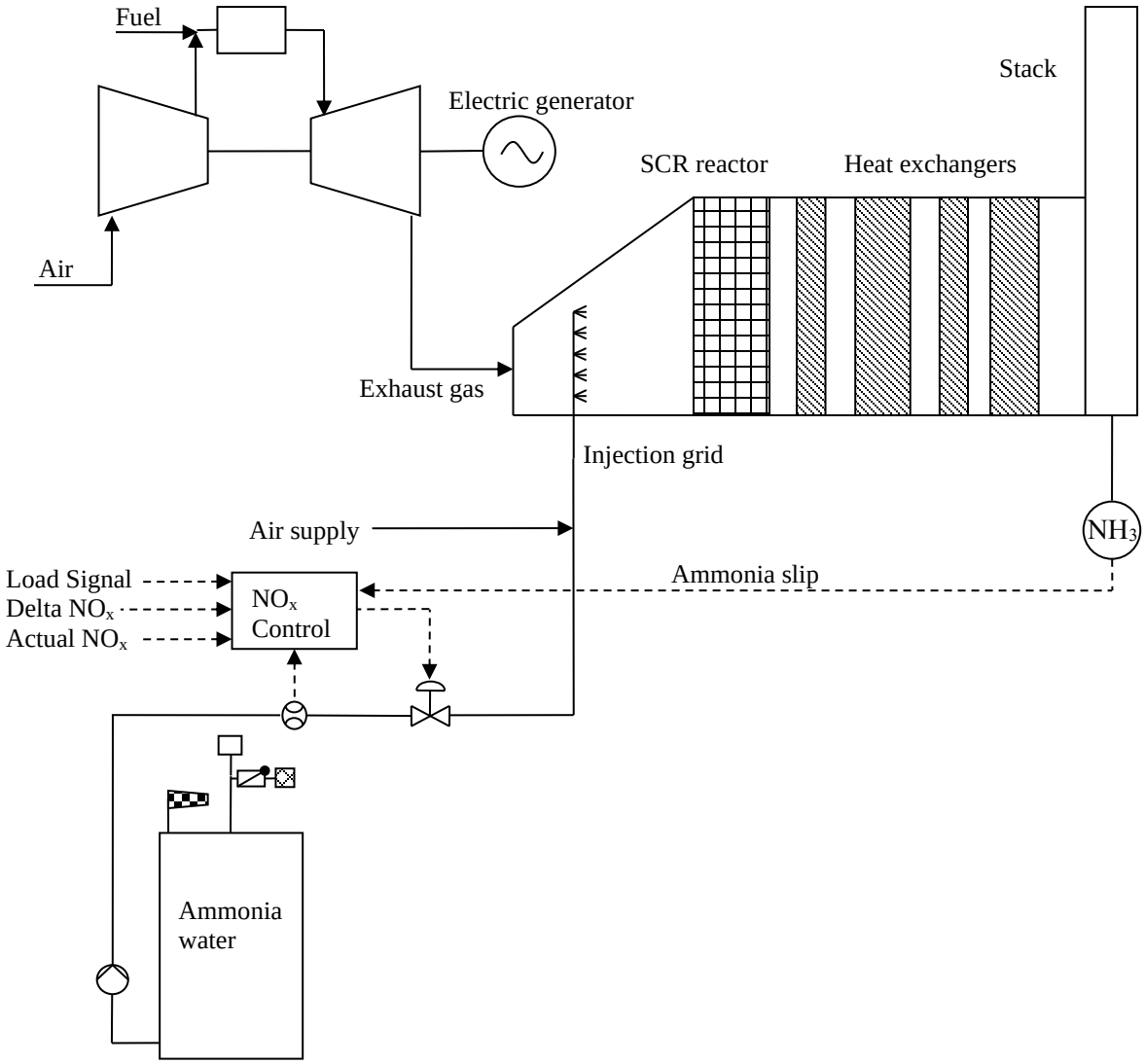

Fig. 3.3 Flow diagram of SCR technology, HRSG boiler [1]

Practical and economic considerations determine the optimum catalyst location and arrangement. Additional concerns affecting the location and arrangement of SCR catalyst involve properly mixing of ammonia and the flue gas. The performance of SCR reactor dependents mainly upon the diffusion surface area, which includes the surface area of both macro and micropores in the catalyst. SCR performance increases with the specific surface area. Since this area is catalyst-specific, it is not a convenient design parameter. A widely used parameter is surface velocity,

which is usually defined as a flue gas flow rate (at the normal condition) divided by the bulk volume of the catalyst. The required space velocity depends upon the catalyst configuration and properties (such as activity, stability, and expected life), NO_x inlet and outlet concentration, flue gas temperature, flue gas SO_2 and SO_3 concentrations, fly ash content and composition and the desired ammonia slip. Space velocity can vary widely depending on these factors.

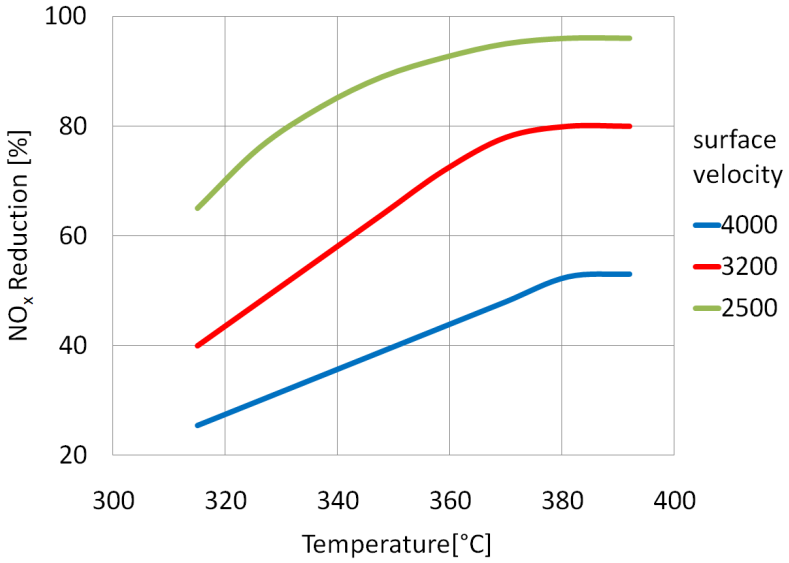

Fig. 3.4 NO_x – reduction depending on surface velocity and temperature [1]

Because catalyst volume is determined based on catalyst-specific space velocity curves, the choice of catalyst type, composition establishes the overall SCR reactor design. The SCR systems are generally based on modular type catalyst configuration using either the parallel plate or honeycomb matrix design. Today, metal oxides and zeolite are used as a catalyst. The catalyst selection must also consider the following operating conditions:

1) High temperatures, which can sinter or reduce catalyst pore volume.
2) Fly ash, which can erode the catalyst.
3) Solid depositions, which can plug pores.
4) Presence of halogen compounds, arsenic, and ammonium bisulphate, which can "poison" the catalyst.
5) Aging of the catalyst, which can decrease catalyst activity.

Guarantees on catalyst life, in general, have increased rapidly and can extend the SCR life by using a catalyst management program. This program is typically based on monitoring the ammonia slip and includes rotation, replacement, and/or adding catalyst layers at scheduled intervals.

Individual catalyst elements are assembled into blocks or modules arranged in horizontal or vertical layers within the reactor on engineered support structures. In large systems, there are several layers with space between each layer for access. The reactor housing is usually oversized

to provide an additional catalyst layer if the catalyst management program requires this. The SCR reactor houses and support the individual catalyst units and includes a sealing system to prevent flue gas from by-passing the catalyst modules. The cross-section area and several catalyst layers are selected to optimise gas velocity, pressure drop, and flow distribution for the required NO_x reduction. In the presence of fly ash, it is preferred to direct the flue gas vertically downward to facilitate the passage of fly ash through the catalyst – the maximum allowable velocity depends on catalyst type and the application.

4 CFD Simulation of SCR

This chapter focuses on the numerical simulation of the SCR process, which can aid to support SCR design. The simplified kinetics model has been proposed for CFD simulation of SCR, and the kinetics model has been designed based on the experimental data available in a scientific article. The reliability of the proposed model has been checked by comparison with the experimental data specified in the task.

4.1 Existing Kinetics Models of SCR

Chemical reactions in the used CFD code are based on the Arrhenius equation, which describes the reaction rate [6].

$$k = A \cdot e^{-\frac{E}{R \cdot T}} \cdot T^{\beta} \left[\frac{(\mathrm{mol} \cdot \mathrm{m}^{-3})^{1-\mathrm{n}} \cdot \mathrm{K}^{\beta}}{\mathrm{s}}\right] \tag{4.1}$$

Where k is reaction rate, A is the pre-exponential factor, E is the activation energy, R is the universal gas constant, T is temperature, β is temperature exponent, n is the sum of the number of reaction orders.

In some proposed research investigations, the SCR process is modelled with a rate order expression. This expression incorporates all the process parameters (temperature and concentrations of ammonia and oxygen) in a simplified and easy to use formula. It can be customised to accurately depict a specific process by performing a comprehensive data set regression analysis.

The selective catalytic reduction rate can be expressed as:

$$r = k \cdot [NH_3]^a \cdot [O_2]^b \cdot [NO]^c \cdot [H_2O]^d \tag{4.2}$$

where k is the reaction rate for temperature T and a, b, c and d are reaction orders of ammonia, oxygen, NO and water.

It means reaction order in equation (4.1) is:

$$n = a + b + c + d \tag{4.3}$$

The rate order with respect to NO has been measured to be $a \cong 1$ by many research groups. The SCR rate dependencies on water concentration can be neglected when oxygen is in excess. The NO concentration is fixed in many studies, while oxygen concentration varies from 0.1% to 3%.

From the elementary equation of SCR eqv. 2.2, it is clear that for SCR four NO molecules require only one molecule of oxygen; hence at the minimum, the oxygen concentration is 12 times the stoichiometric value or a 1200% excess. Hence the water concentration would not affect the SCR rate, i.e., $d = 0$.

In research work [13], rate constants and ammonia and oxygen exponents for V based catalysts are discussed. The rate order expression is given by:

$$r = k \cdot [NH_3]^{0.2427} \cdot [O_2]^{0,1133} \cdot [NO]^1 \cdot [H_2O]^0 \qquad (4.4)$$

The ammonia exponent is 0,2427 that indicates that the reaction rate increases with inlet ammonia concentration. In contrast, the oxygen exponent is comparable at 0,1133, indicating a positive dependence of reaction rate on inlet oxygen concentration.

Experimental research [10] discussed parameters of NO reduction on TiO – V catalyst. Parameters for reaction rate k can be estimated based on experimental data.

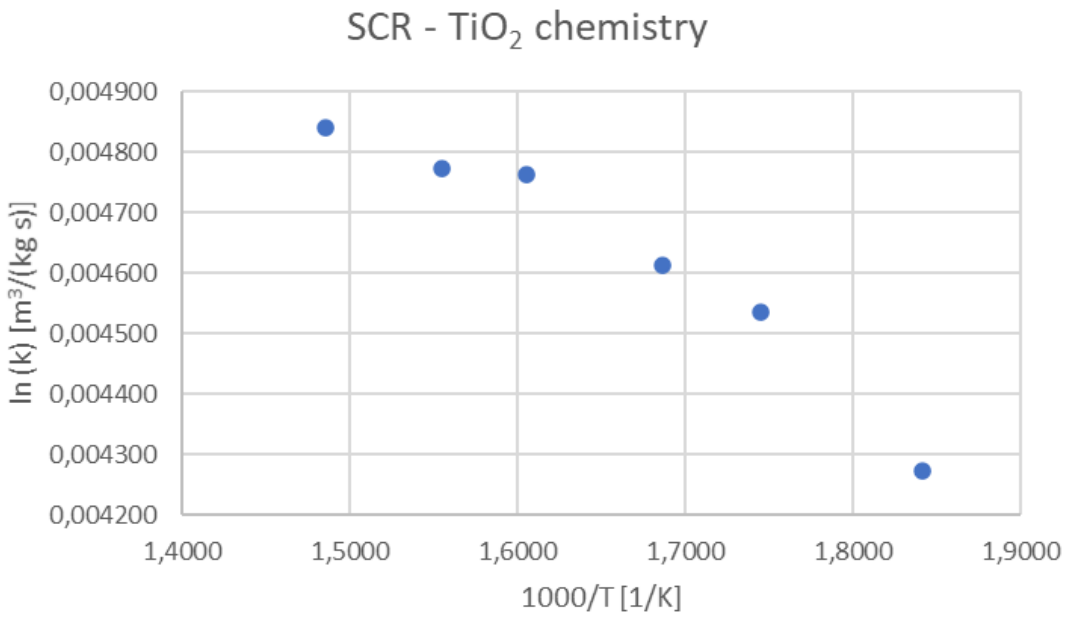

Fig. 4.1 Reaction rate k as a function of reciprocal temperature [10]

Pre-exponential factor A, activation energy E and temperature exponent β was expressed based on regression analysis of experimental data. The reaction rate expression is given by $A = 1{,}160417$; $E = 108828\ \left[\frac{J}{kmol}\right]$ and $\beta = -0{,}019$

4.2 Simplified Kinetics Model

The reduced kinetics model does not work well over a wide range of operating conditions. The simplified model describes only the basic processes of SCR. The practical simulation of SCR with a simplified chemical kinetics model is instrumental to the design of SCR technology and main design parameters evaluation, like NO_x reduction, ammonia slip, consumption of reagent etc.

Primary thermal dissociation of urea or ammonia is neglected. Only pure ammonia is injected into flue gas flow, a mixture of pure ammonia with flue gas exhausted from the boiler and used as a transport medium.

NO and reduction process is described by following reaction (4.5). This reaction specifies the conversion of NO into nitrogen N_2 and water H_2O. This reaction represents the positive influence of the SCR method on NO_x pollutant concentration in the flue gas.

$$1\ NH_3 + 1\ NO\ +\ 0{,}25\ O_2 \rightarrow 1\ N_2 + 1{,}5\ H_2O \tag{4.5}$$

One problem of SCR is the conversion of SO_2 to SO_3. Conversion of SO_2 is described by the following reaction (4.6):

$$SO_2 + 0{,}5\ O_2 \rightarrow SO_3 \tag{4.6}$$

A secondary positive of the SCR method is the reduction of CO, which is partially reduced by following reaction (4.7). This reaction describes the combustion of CO.

$$CO + 0{,}5\ O_2 \rightarrow CO_2 \tag{4.7}$$

The proposed mechanism does not include Ammonia radical $NH_2 \cdot$ that means the problematic non-stable transitional material is not necessary to be specified.

The proposed kinetics model of SCR was checked by the comparison with task experiments data, which are available in design parameter data of SCR. Reduction of NO_x depending on catalyst parameters and count of layers confronted with design parameter data of SCR, which are generally validated.

The constant improvement of computer resources is providing a continuous increase in computational fluid dynamics in various branches of engineering. Nowadays, CFD is a support to optimise aerodynamic equipment and can be used in the simulation of typical industrial processes, such as SCR. The main advantage of CFD codes is their capability to describe complex processes in detail, e.g., detail simulation of reagent injection in combustion chamber via AIG.

The simplified kinetics model was tested through CFD simulation of the simply real-size combustion chamber in typical conditions, such as the real composition of flue gas, injection, etc.

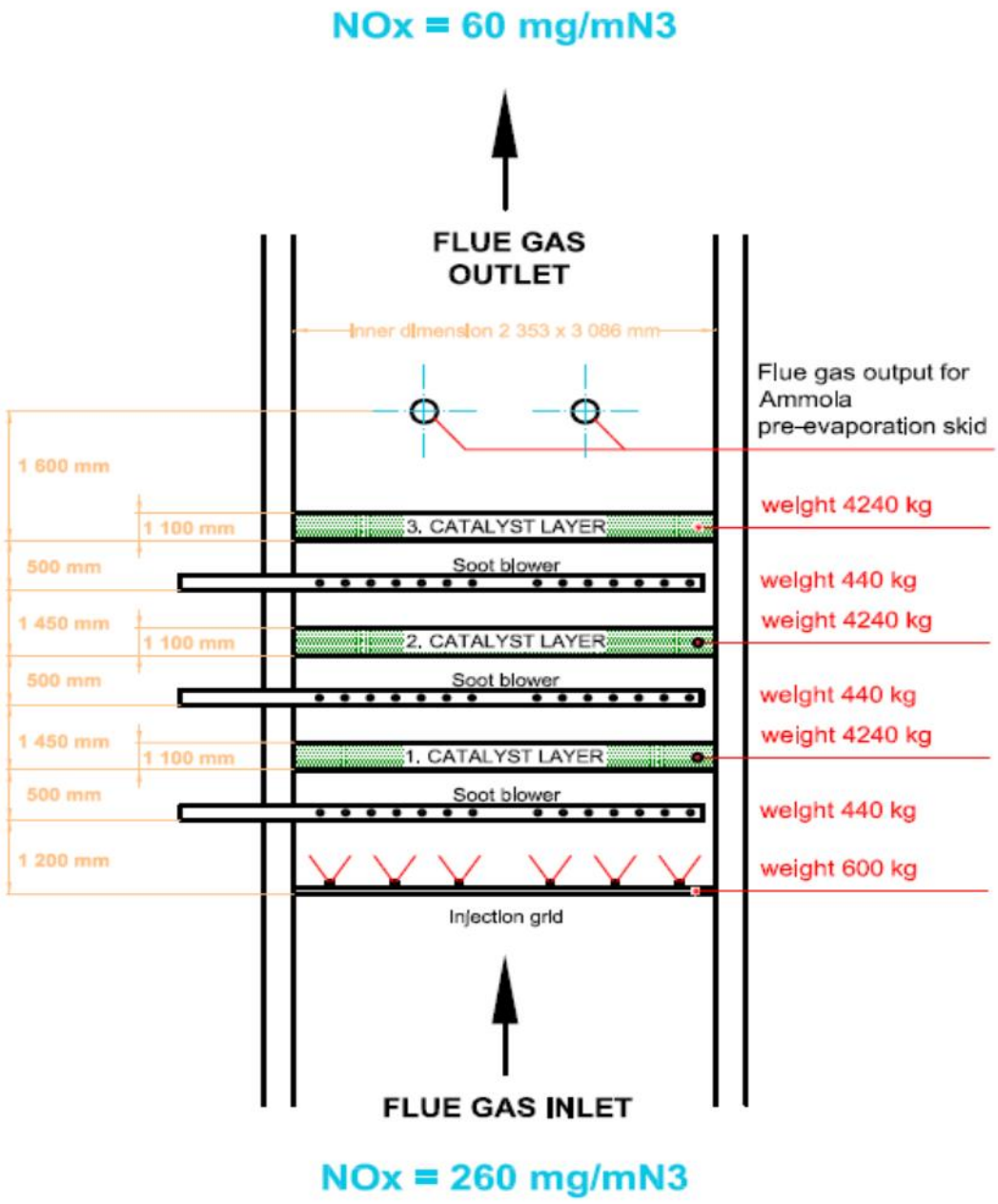

Fig. 4.2 Basic sketch of the test reactor

The mathematical background of multiphase flow with chemical reaction is discussed in several books, which deal with numerical simulation of the turbulent fluid flow.

At first, it has investigated the influence of coupling the CFD with the simplified kinetics model previously discussed. The effect of turbulence was modelled using standard k-ε approaches. The classical approach to model turbulent flows is based on averages of the Navier-Stokes equations. These are commonly called Reynolds Averaged Navier-Stokes equations (RANS). The simplest

model for turbulent flow is *k-ε*. Even though it certainly is the best compromise for engineering design using the RANS approach.

For non-constant density flows, the Navier-Stokes equations are written in the conservative form:

Momentum equations

$$\frac{\partial(\rho \cdot v_i)}{\partial t} + \frac{\partial(\rho \cdot v_i \cdot v_j)}{\partial x_j} = \\ = -\frac{\partial p}{\partial x_i} + \frac{\partial}{\partial x_j} \cdot \tau_{ij} + \rho \cdot \delta_{i3} \cdot g + \rho \cdot f_c \cdot \varepsilon_{ij3} \cdot v_j \\ \tau_{ij} = \mu \cdot \left(2 \cdot S_{ij} - \frac{2}{3}\delta_{ij}\frac{\partial v_i}{\partial x_j}\right);\ S_{ij} = \frac{1}{2}\left(\frac{\partial v_i}{\partial x_j} + \frac{\partial v_j}{\partial x_i}\right) \quad (4.8)$$

Continuity equation

$$\frac{\partial \rho}{\partial t} + \frac{\partial(\rho \cdot v_j)}{\partial x_j} = 0 \quad (4.9)$$

where v is velocity (u, v, w), t is time, x is coordinate (x, y, z), p is static pressure, ρ is density, μ is dynamic viscosity, τ_{ij} is the viscous stress tensor, S_{ij} is the rate of strain tensor, g is gravity acceleration, δ_{i3} is Kronecker symbol ($\delta_{ij} = 1$ for $i = j$, $\delta_{ij} = 0$ for $i \neq j$), ε_{ijk} is unit tensor ($\varepsilon_{ijk} = 1$ for $ijk = 123,231,312$, $\varepsilon_{ijk} = -1$ for $ijk = 321,213,132$, $\varepsilon_{ijk} = 0$ for other combination of ijk).

In equation (4.8), the two left terms on the left-hand side represent the local rate of change and convection of the momentum, respectively. The first term on the right side is the pressure gradient, and the second term represents molecular transport due to viscosity. The third term represents the buoyant effect, and the fourth term represents the Coriolis effect. Using Reynolds averaging on equations (4.8) and (4.9), one obtains averaged equations.

Averaged momentum equations

$$\frac{\partial(\rho \cdot \overline{v_i})}{\partial t} + \frac{\partial\left(\rho \cdot \overline{v_i} \cdot \overline{v_j}\right)}{\partial x_j} + \frac{\partial\left(\rho \cdot \overline{v_i' \cdot v_j'}\right)}{\partial x_j} =$$
$$= -\frac{\partial \bar{p}}{\partial x_i} + \frac{\partial}{\partial x_j} \cdot \overline{\tau_{ij}} + \rho \cdot \delta_{i3} \cdot g + \rho \cdot f_c \cdot \varepsilon_{ij3} \cdot \overline{v_j} \qquad (4.10)$$
$$\overline{\tau_{ij}} = \mu \cdot \left(2 \cdot \overline{S_{ij}} - \frac{2}{3} \cdot \delta_{ij} \cdot \frac{\partial \overline{v_i}}{\partial x_j}\right); \overline{S_{ij}} = \frac{1}{2} \cdot \left(\frac{\partial \overline{v_i}}{\partial x_j} + \frac{\partial \overline{v_j}}{\partial x_i}\right)$$

Continuity equation

$$\frac{\partial \rho}{\partial t} + \frac{\partial\left(\rho \cdot \overline{v_j}\right)}{\partial x_j} = 0 \qquad (4.11)$$

Equation (4.10) is like (4.8) except for the third term of the right side of the equation. The new term $\left(\rho \cdot \overline{v_i' \cdot v_j'}\right)$ is called Reynolds stress tensor. This tensor is unknown and represents the first closure problem for turbulence modelling. It is possible to derive the equation for the six components of the Reynolds stress tensor. Although the Reynolds stress model contains a complete description of the physics, it is not yet widely used in turbulent combustion. Many industrial codes still rely on the k-ε model, which introduces the assumption of isotropy by using an eddy viscosity. It is known that turbulence becomes isotropic at the small scales, but this does not necessarily apply to the large scale at which the averaged quantities are defined. The *k-*ε model is based on equations where the turbulent transport is diffusive and therefore is more easily handled by numerical method than the Reynolds stress equation. This is probably the most important reason for its wide use in many codes. An important simplification is obtained by introducing the eddy viscosity μ_t, which lead to the following expression for the Reynolds stress tensor.

$$-\rho \cdot \overline{v_i} \cdot \overline{v_j} = \mu_t \cdot \left(2 \cdot \overline{S_{ij}} - \frac{2}{3} \cdot \delta_{ij} \cdot \frac{\partial \overline{v_i}}{\partial x_j}\right) - \frac{2}{3}\delta_{ij} \cdot \rho \cdot k \qquad (4.12)$$

Where k is turbulent kinetic energy.

Turbulent kinetic energy and eddy dissipation are related to turbulent viscosity by equation.

$$\mu_t = \rho \cdot C_\mu \cdot \frac{k^2}{\varepsilon} \qquad (4.13)$$

Where ε is eddy dissipation and C_μ is constant.

The introduction of variables k, ε requires that modelled equations are available for these quantities.

Turbulent kinetic energy

$$\frac{\partial(\rho \cdot k)}{\partial t} + \frac{\partial\left(\rho \cdot \overline{v_j} \cdot k\right)}{\partial x_j} = \\ = \frac{\partial}{\partial x_j} \cdot \left(\left(\mu + \frac{\mu_t}{\sigma_k}\right) \cdot \frac{\partial k}{\partial x_j}\right) + G_k - G_b - \rho \cdot \varepsilon - Y_M \tag{4.14}$$

Turbulent eddy dissipation

$$\frac{\partial(\rho \cdot \varepsilon)}{\partial t} + \frac{\partial\left(\rho \cdot \overline{v_j} \cdot \varepsilon\right)}{\partial x_j} = \\ = \frac{\partial}{\partial x_j} \cdot \left(\left(\mu + \frac{\mu_t}{\sigma_\varepsilon}\right) \cdot \frac{\partial \varepsilon}{\partial x_j}\right) + C_{\varepsilon 1} \frac{\varepsilon}{k} \cdot (G_k + C_{3\varepsilon} \cdot G_b) - C_{2\varepsilon} \cdot \rho \cdot \frac{\varepsilon^2}{k} \tag{4.15}$$

Where G_k is the production of turbulent kinetic energy, G_b is the generation of turbulence due to buoyancy, and Y_M is the production of turbulence due to compressibility.

$$G_k = \mu_t \cdot \left(\frac{\partial \overline{v_j}}{\partial x_l} + \frac{\partial \overline{v_l}}{\partial x_j}\right) \cdot \frac{\partial \overline{v_j}}{\partial x_l}$$

$$G_b = -g_j \cdot \frac{\mu_t}{\rho \cdot \sigma_h} \cdot \frac{\partial \rho}{\partial x_j} \tag{4.16}$$

$$\sigma_h = \frac{\mu_t}{\lambda_t} \cdot c_p$$

$$Y_M = 2 \cdot \rho \cdot \varepsilon \cdot \frac{k}{\gamma \cdot R \cdot T}$$

Where σ_h is Turbulent Prandtl number, λ_t is turbulent thermal conductivity, $and\ c_p$ is specified heat capacity.

In equations (4.14) and (4.15), the two teem on the left side represent local rate and convection, respectively. The first term on the right side represents turbulent transport, the second is turbulent production, and the third is turbulent dissipation.

4.3 CFD Simulation of Real SNCR in Real Boiler

Real SCR technology is based on reagent injection into the combustion chamber of a boiler, as mentioned above.

The SCR technology is a relatively simple technological unit, but it includes some important parts, which dominantly influence the effective efficiency of NO_x reduction. One of the important parts is injection grid AIG. The AIG is located upstream first catalyst layer. The main parameter of the AIG is the homogenous penetration of flue gas by the reagent. The problem of jet penetration and mixing in turbulent crossflow is relevant in many industrial applications, and several researchers have studied it. The characteristic mixing time is not exactly the time required for molecular mixing of primary crossflow with the lateral jet stream. This is worth mentioning that the relations usually employed to calculate the jet length penetration and then characteristic mixing time is often derived under the free jet assumption, neglecting the crossflow conditions because the measuring of the injection process is not realisable in situ.

Numerical simulation of the SCR includes a problematic definition of inlet boundary conditions. These boundary conditions must include temperature, velocity, O_2, N_2, CO_2, NO, CO, SO_2, SO_3 and H_2O. As a source of boundary conditions can be used CFD simulation of combustion process or measured field data. However, simulation of the combustion process in the combustion chamber is very complicated and time-consuming. If the profiles of boundary condition variables are unknown for a specific unit, measured profiles from another unit can be applied if the other unit is sufficiently similar in geometry and firing conditions. The mass flow, temperature, and concentration of all species were specified in task data, so the full combustion model was not necessarily performed.

SCR model was tested on the geometry of the coal combustion boiler and project design data specified by the catalyst manufacturer. The boiler is a waste incineration type and, as a fuel, is used municipal waste. The geometry of the combustion chamber part with catalyst was created according to drawing documentation (see Fig. 4.3). Domain inlet is located downstream of the main combustion zone in the second draft. The domain includes an ash hopper too. The domain outlet is located downstream of the last layer of the catalyst. All heat exchangers and soot blowers were neglected.

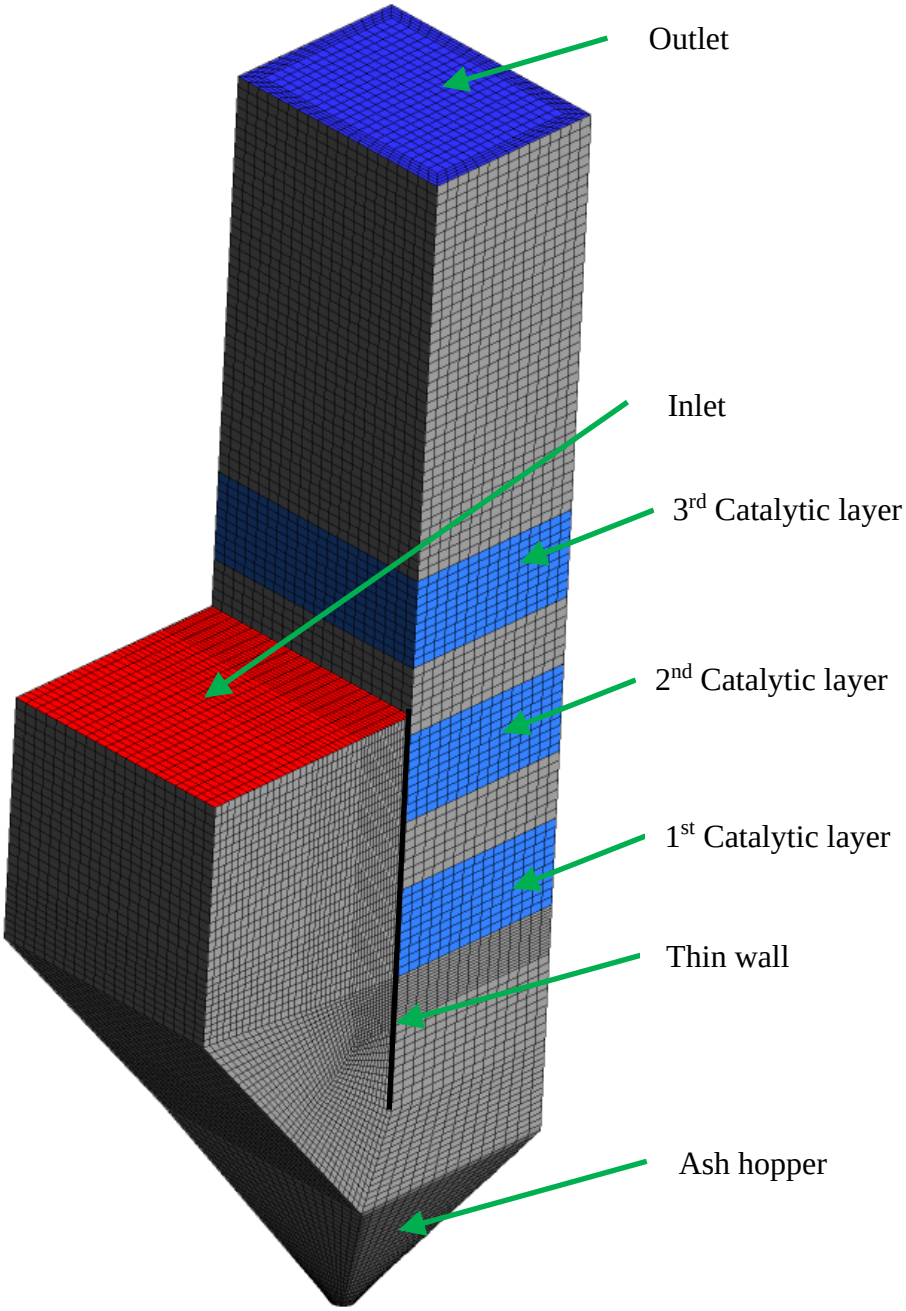

Fig. 4.3 Geometry of boiler

This geometry was used for CFD simulation of the SCR process because the temperature Window 320–400°C, which is an ideal operational temperature for TiO_2 catalyst type.

CFD simulations were compared with the results of design data. The CFD simulations and experimental measurements were performed for boiled load 100% (30 t_{steam}/h), it means $Q_{flue\ gas}$ = 53 340 m_N^3/h and temperature $t_{flue\ gas}$ = 400°C. CFD simulation was performed for three variants, one two and three layers of catalyst, specified in task data, and ideal penetration of reagent in the flue gas was assumed. Then variant with three layers was simulated with real AIG, which means real reagent penetration in the flue gas.

4.4 Results

Results of CFD simulation were compared with task data. The main parameters were reduction of NO, pressure drop Δp and next reduction of CO, conversion of SO_2 to SO_3. The concentration of all species was calculated as an area-weighted average up and a downstream active catalytic layer or layers. The main results are well-arranged in the next tables.

4.4.1 Results – ideal AIG

Tab. 4.1 Comparison of task data with CFD simulation, NO reduction

		NO_{inlet}	NO_{outlet}	Reduction	Error
		[mg·m_N^{-3}]		[%]	[%]
Var 1	Data	260	225,0	13,5	-1,2
One catalyst layer	CFD	260	225,4	13,3	
Var 2	Data	260	120,0	53,8	-1,2
Two catalyst layers	CFD	260	121,7	53,2	
Var 3	Data	260	60,0	76,9	-1,8
Three catalyst layers	CFD	260	63,2	75,7	

Tab. 4.2 Comparison of task data with CFD simulation, CO reduction

		CO_{inlet}	CO_{outlet}	Reduction	Error
		[mg·m_N^{-3}]		[%]	[%]
Var 1	Data	50	N/A	N/A	N/A
One catalyst layer	CFD	50	36,9	26,2	
Var 2	Data	50	N/A	N/A	N/A
Two catalyst layers	CFD	50	24,7	45,2	
Var 3	Data	50	ca. 20,0	ca. 60,0	-0,8
Three catalyst layers	CFD	50	20,2	59,5	

Tab. 4.3 Comparison of task data with CFD simulation, conversion of SO_2 to SO_3

		SO_{2inlet}	$SO_{2outlet}$	Conversion to SO_3	Error
		[mg·m_N^{-3}]		[%]	[%]
Var 1	Data	857	N/A	N/A	N/A
One catalyst layer	CFD	857	853,4	0,4	
Var 2	Data	857	N/A	N/A	N/A
Two catalyst layers	CFD	857	849,8	0,8	
Var 3	Data	857	ca. 848	ca. 1,0	+25,3
Three catalyst layers	CFD	857	846,3	1,3	

Tab. 4.4 Comparison of task data with CFD simulation, an increase of SO_3

		SO_{3inlet}	$SO_{3outlet}$
		[mg·m$_N^{-3}$]	
Var 1 One catalyst layer	CFD	0	4,8
Var 2 Two catalyst layers	CFD	0	9,5
Var 3 Three catalyst layers	CFD	0	13,1

Pressure drop is specified as a rough estimated value; thus, it cannot be well compared with CFD results. The support construction for catalyst layers and soot blowers were neglected in geometry, so pressure drop calculated by CFD represents only friction loss in catalyst layer or layers (3 x 3 mm ducts).

Tab. 4.5 Comparison of task data with CFD simulation, pressure drop.

		Δp
		[mbar]
Var 1 One catalyst layer	Data	ca. 5,0
	CFD	3,1
Var 2 Two catalyst layers	Data	ca. 7,0
	CFD	6,3
Var 3 Three catalyst layers	Data	ca. 10,0
	CFD	9,4

The next chart illustrates the decrease of NO downstream of the catalyst with respect to the count of catalyst layers. The chart compares the results of CFD with the task.

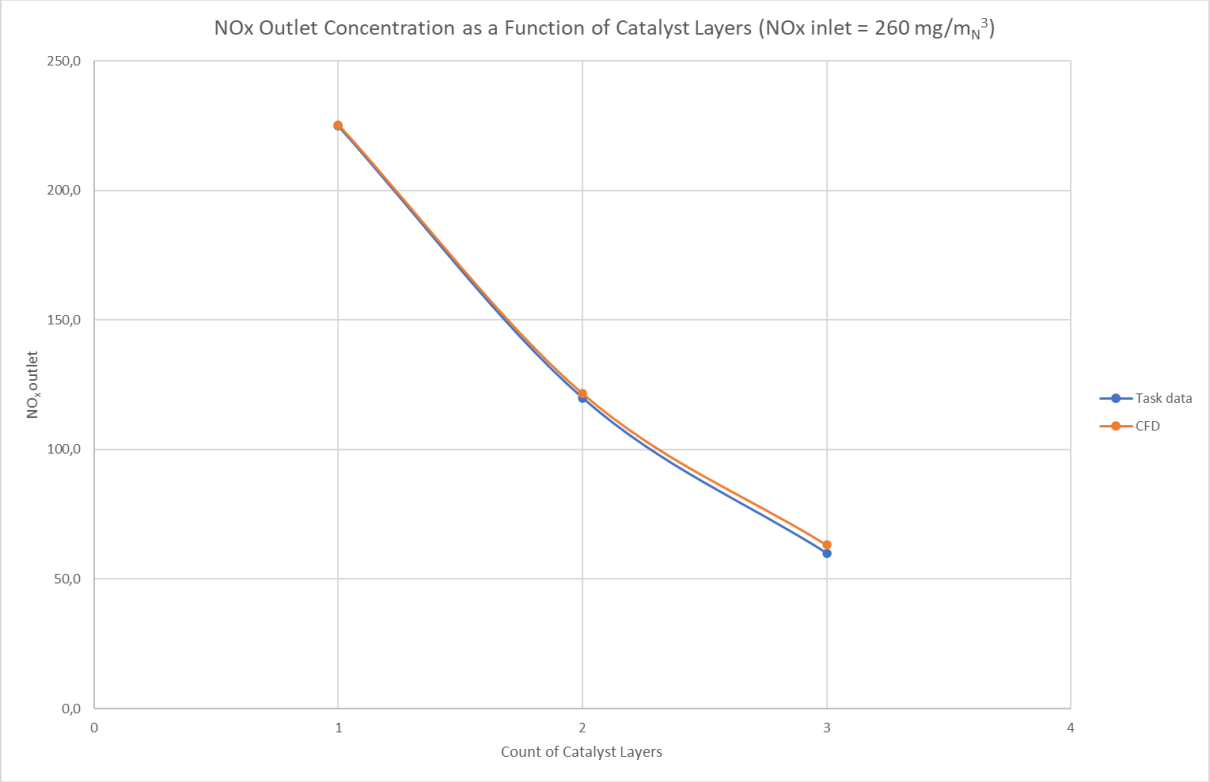

Fig. 4.4 Concentration of NO_{outlet} as a function of catalyst layers

The following charts illustrate the concentration of NO, CO, SO_3 along the streamline. The concentration of species is calculated as an area-weighted average across the streamline, which is identical to the duct axis. Charts represent the effect of multiple catalyst layers, so for example, we can see a decrease of NO across the stream of flue gas flowing through individual catalyst layers.

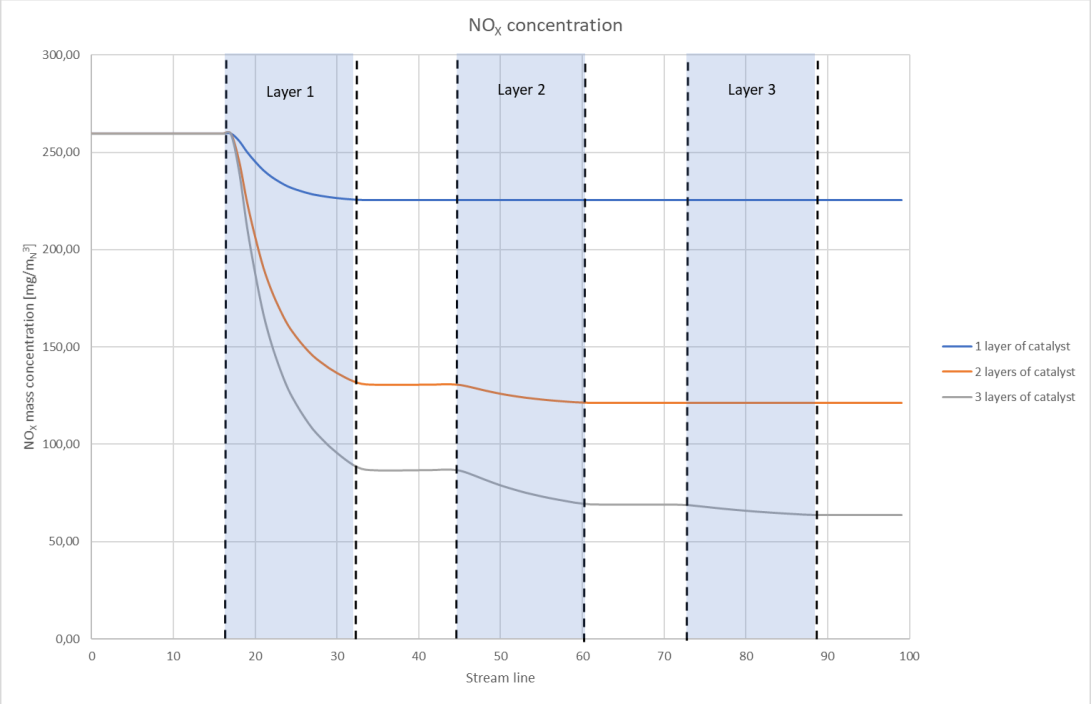

Fig. 4.5 Concentration of NO along the streamline

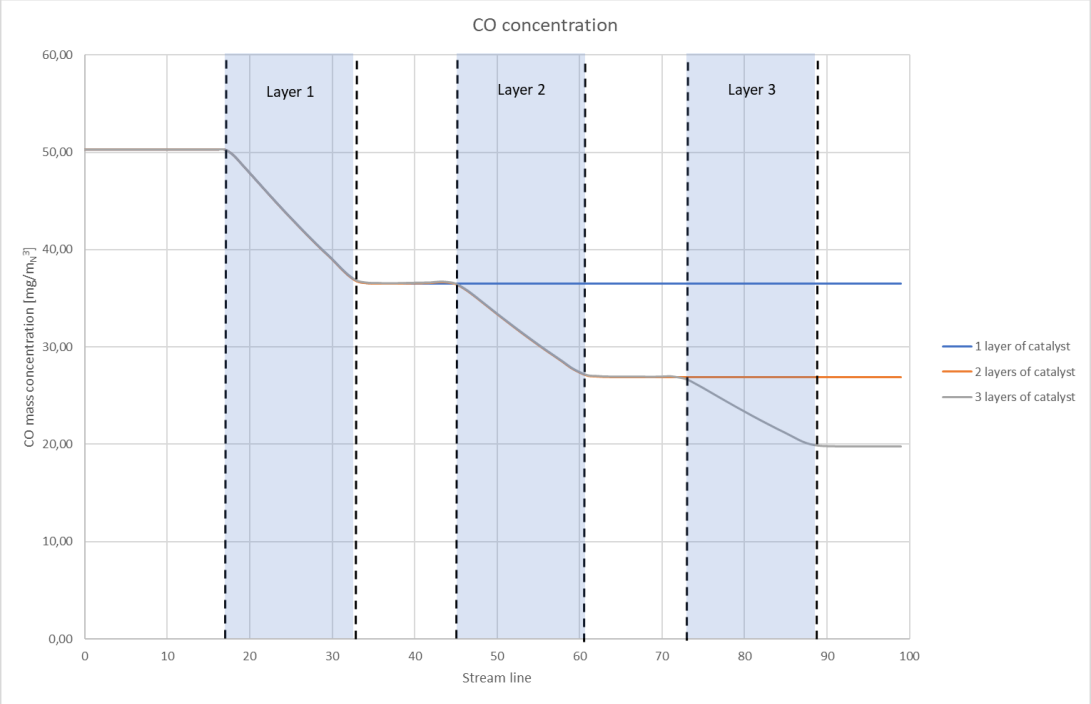

Fig. 4.6 Concentration of CO along the streamline

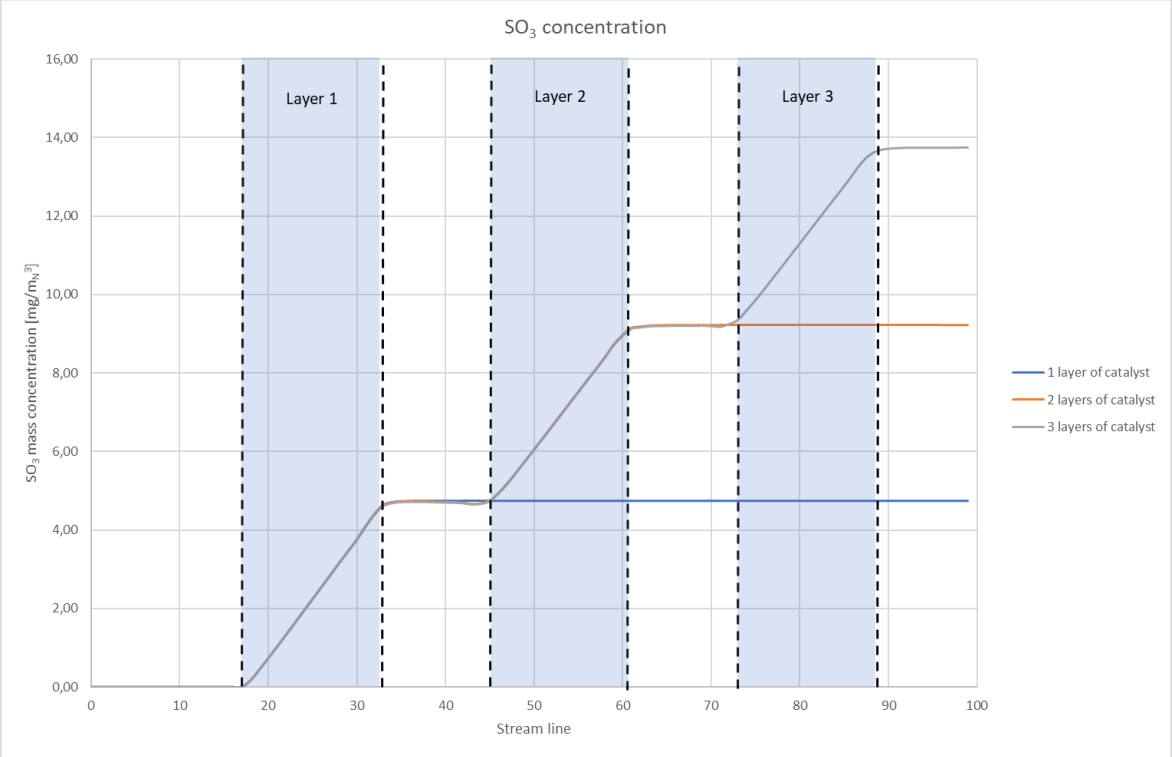

Fig. 4.7 Concentration of SO_3 along the streamline

4.4.2 Results – real AIG

As a second, the effectivity of AIF was analysed. The real AIG was added to the boiler geometry, and an inlet for individual pipelines of AIG was specified. AIG is designed as a pipe with dozens of holes. The holes are injection nozzles of reagent. The AIG was sketched according to drawing documentation.

Flue gas is sucked from the combustion chamber downstream of the catalyst. Then, the reagent (Ammonia water) is evaporated in a mixing chamber and mixed with sucked flue gas. A mixture of gaseous ammonia and flue gas is handled to the AIG by two blowers. Real AIG influences the local flow field by producing turbulent kinetic energy by mixing two perpendicular flows, the main flow of flue gas and a perpendicular jet of a mixture of flue gas and gaseous ammonia NH_3. The second source of turbulent kinetic energy is flowing around the cylinder; it means flow around individual pipes of AIG. Produced turbulence ensures the mixing of flue gas with gaseous ammonia NH_3. Only var3 (three layers of catalyst) with real AIG was simulated and compared with CFD var3 with an ideal injection of reagent. This comparison shows the effect of AIG, and the influence of NO reduction by the effectivity of injection can be estimated.

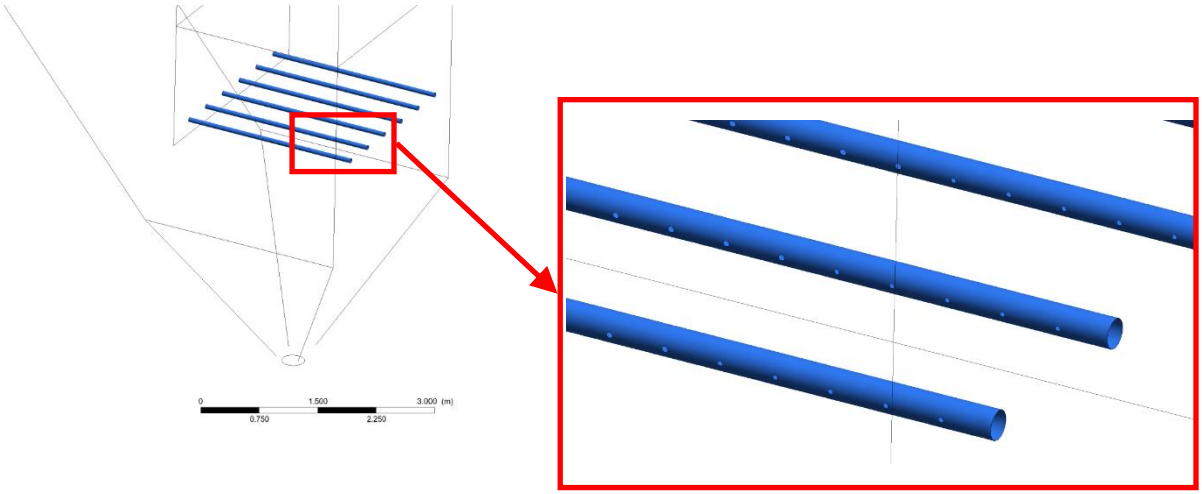

Fig. 4.8 Detail of AIG geometry

A comparison of simulation with real AIG and the ideal case is arranged in the following tables. Variant with ideal penetration of flue gas by reagent is taken as a reference value for specification of the effect of real AIG. The transport gas effect influences the comparison. It means that the ideal AIG does not respect the composition of flue gas that is sucked from the combustion chamber, and it is the handling medium for the transport of reagent to the AIG and combustion chamber, respectively.

Tab. 4.6 Comparison of real and ideal AIG, NO reduction

	NO_{inlet}	NO_{outlet}	Reduction	Influence
	[mg·m$_N^{-3}$]		[%]	
Ideal mixing	260	63,2	75,7	ref.100 %
Real AIG	260	91,8	64,7	-14,5 %

Tab. 4.7 Comparison of real and ideal AIG, CO reduction

	CO_{inlet}	CO_{outlet}	Reduction	Influence
	[mg·m$_N^{-3}$]		[%]	
Ideal mixing	50	20,2	59,5	ref.100 %
Real AIG	50	19,8	60,4	+1,5 %

Tab. 4.8 Comparison of real and ideal AIG, CO reduction

	SO_{2inlet}	$SO_{2outlet}$	Conversion to SO_3	Influence
	[mg·m$_N^{-3}$]		[%]	
Ideal mixing	857	846,3	1,3	ref.100 %
Real AIG	857	846,8	1,3	±0 %

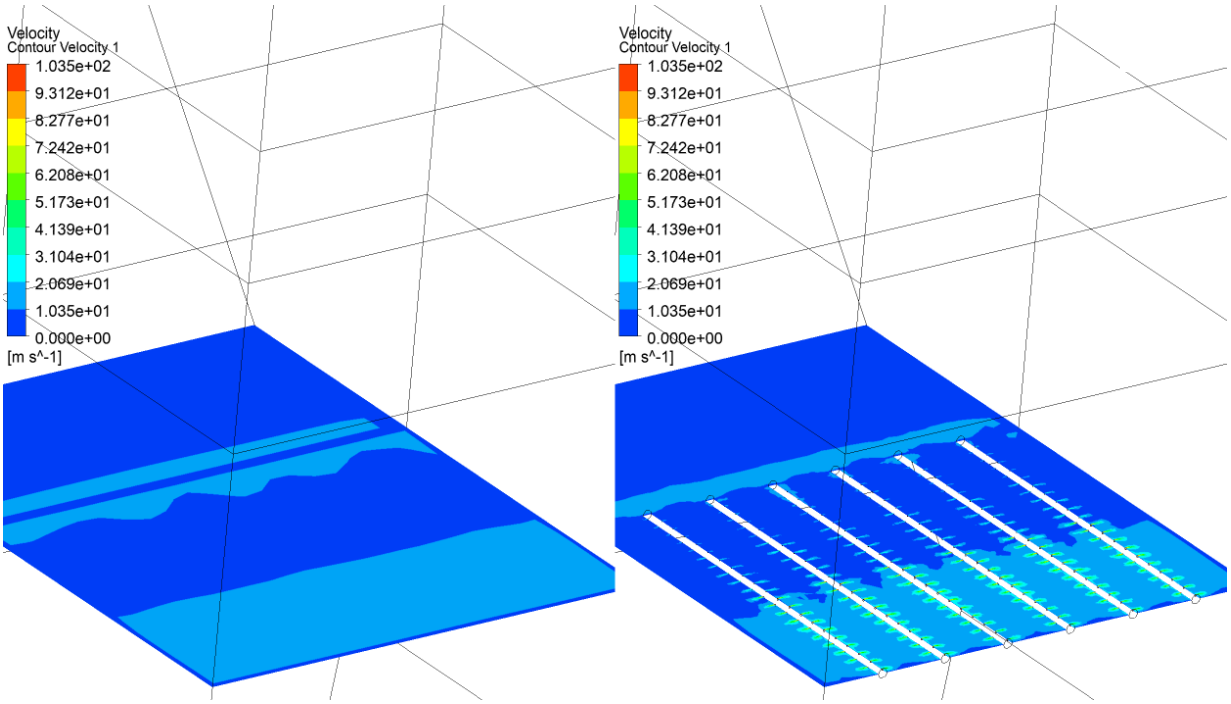

Fig. 4.9 Comparison of velocity at AIG level, Ideal – left, Real – right

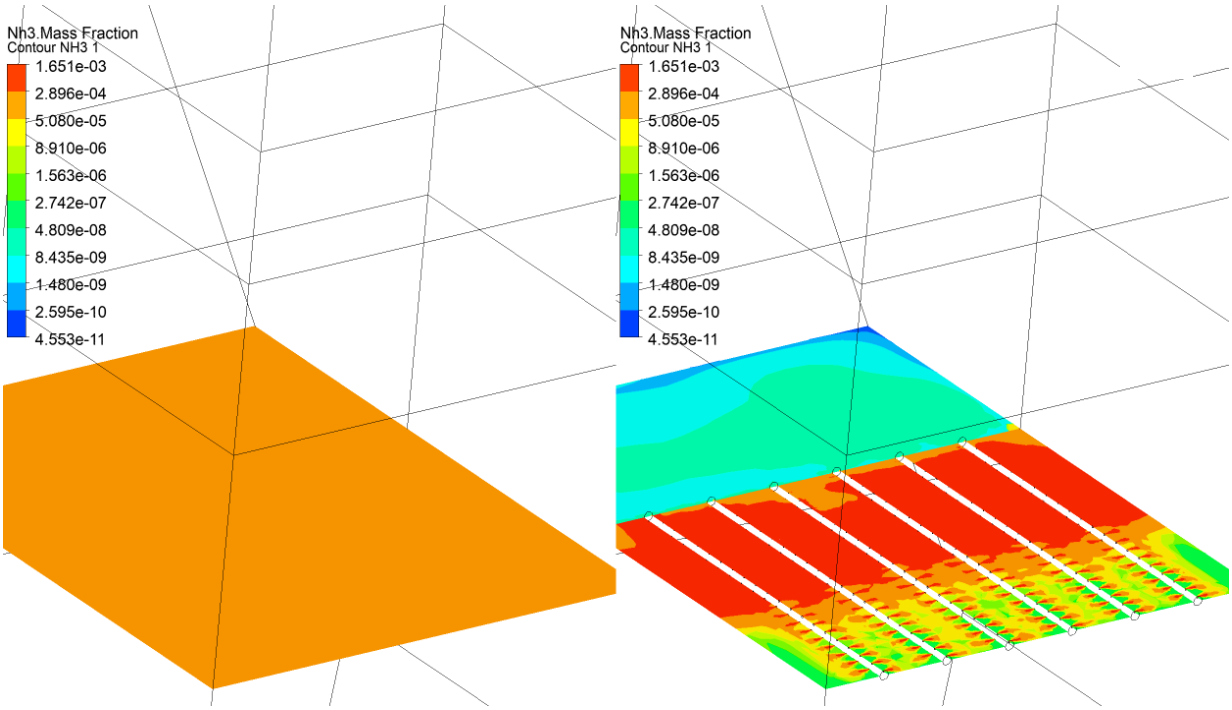

Fig. 4.10 Comparison of NH_3 concentration at AIG level, Ideal – left, Real – right

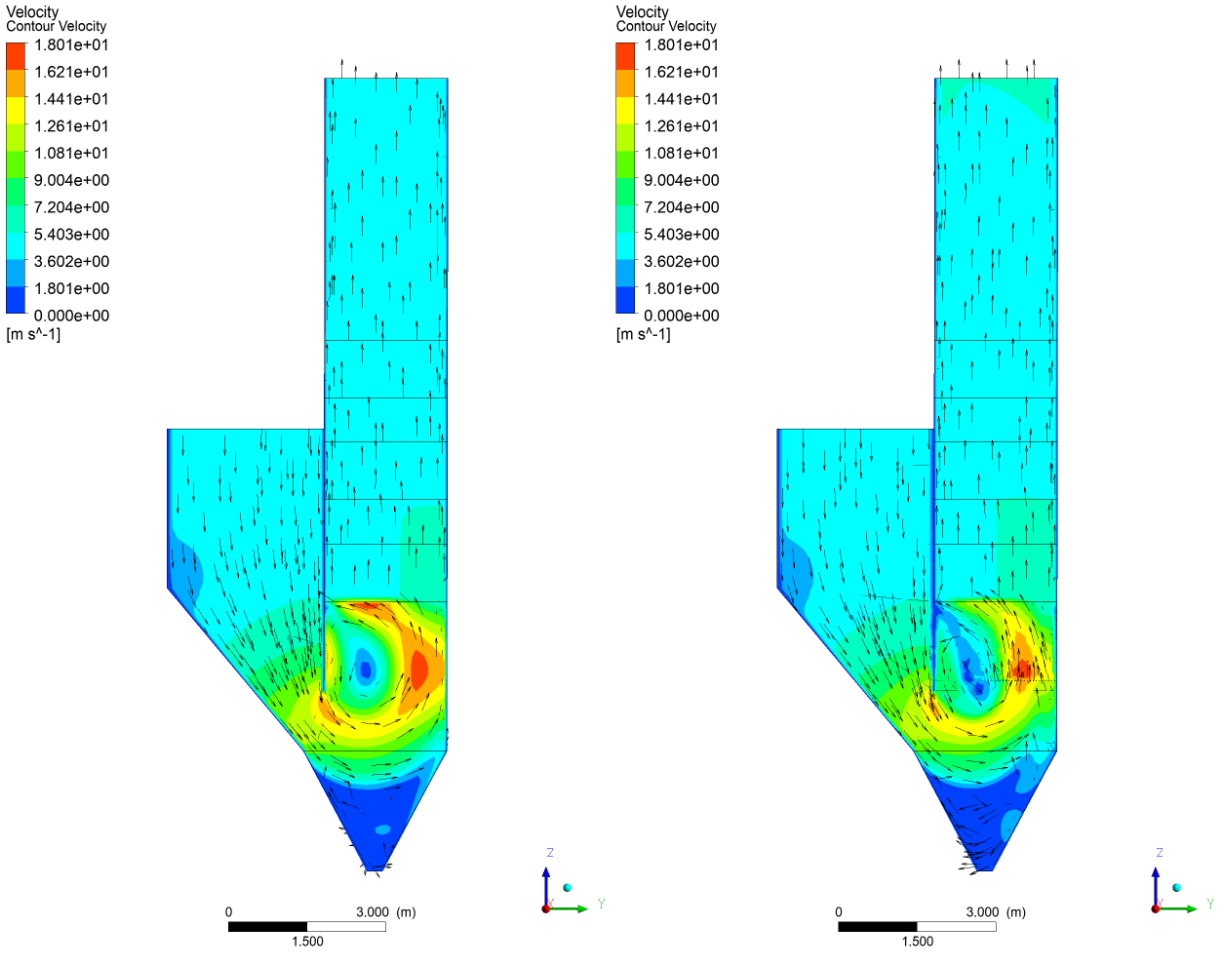

Fig. 4.11 comparison of velocity magnitude, vertical cross-section: Ideal – left, Real – right

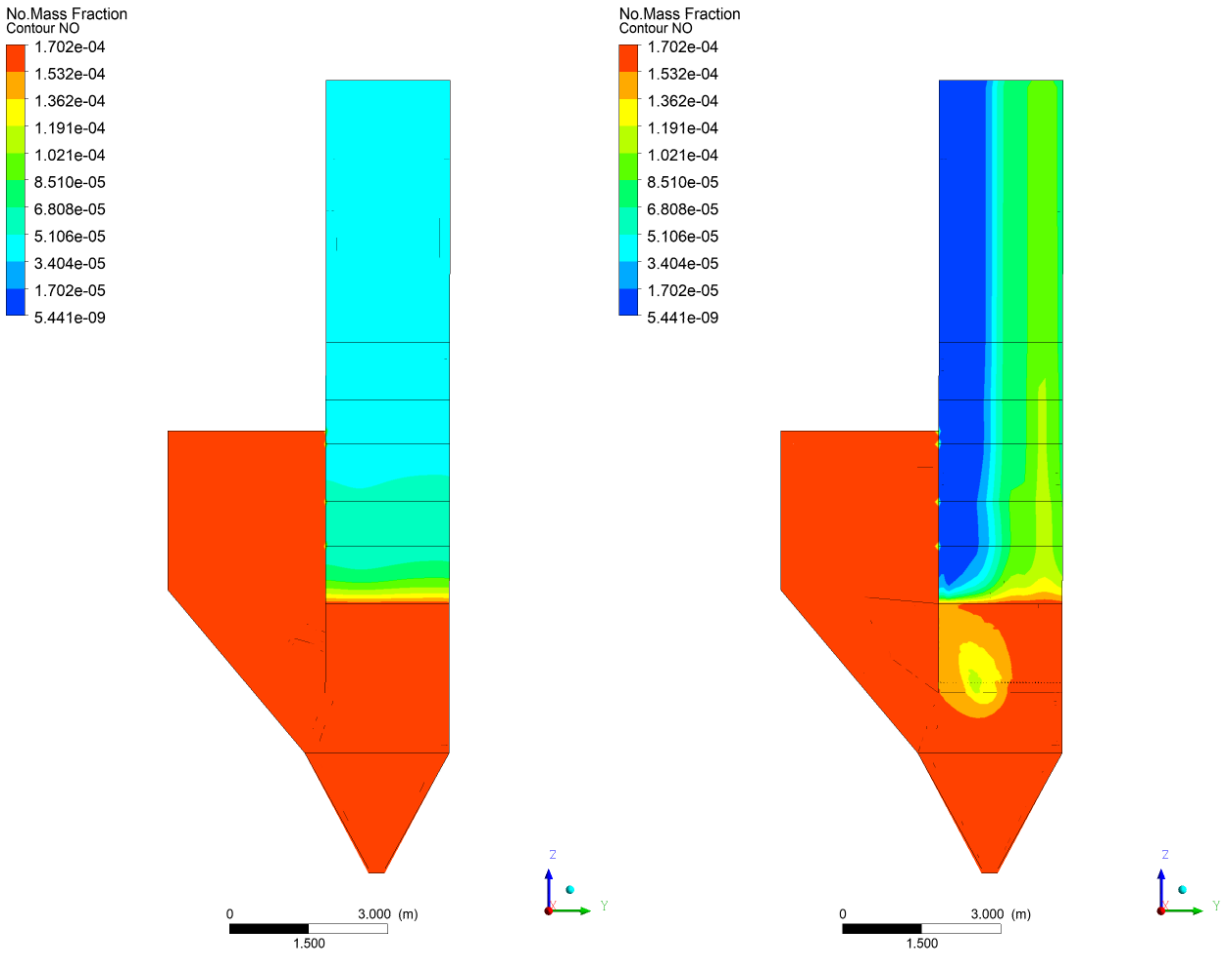

Fig. 4.12 Comparison of NO concentration, vertical cross-section: Ideal – left, Real – right

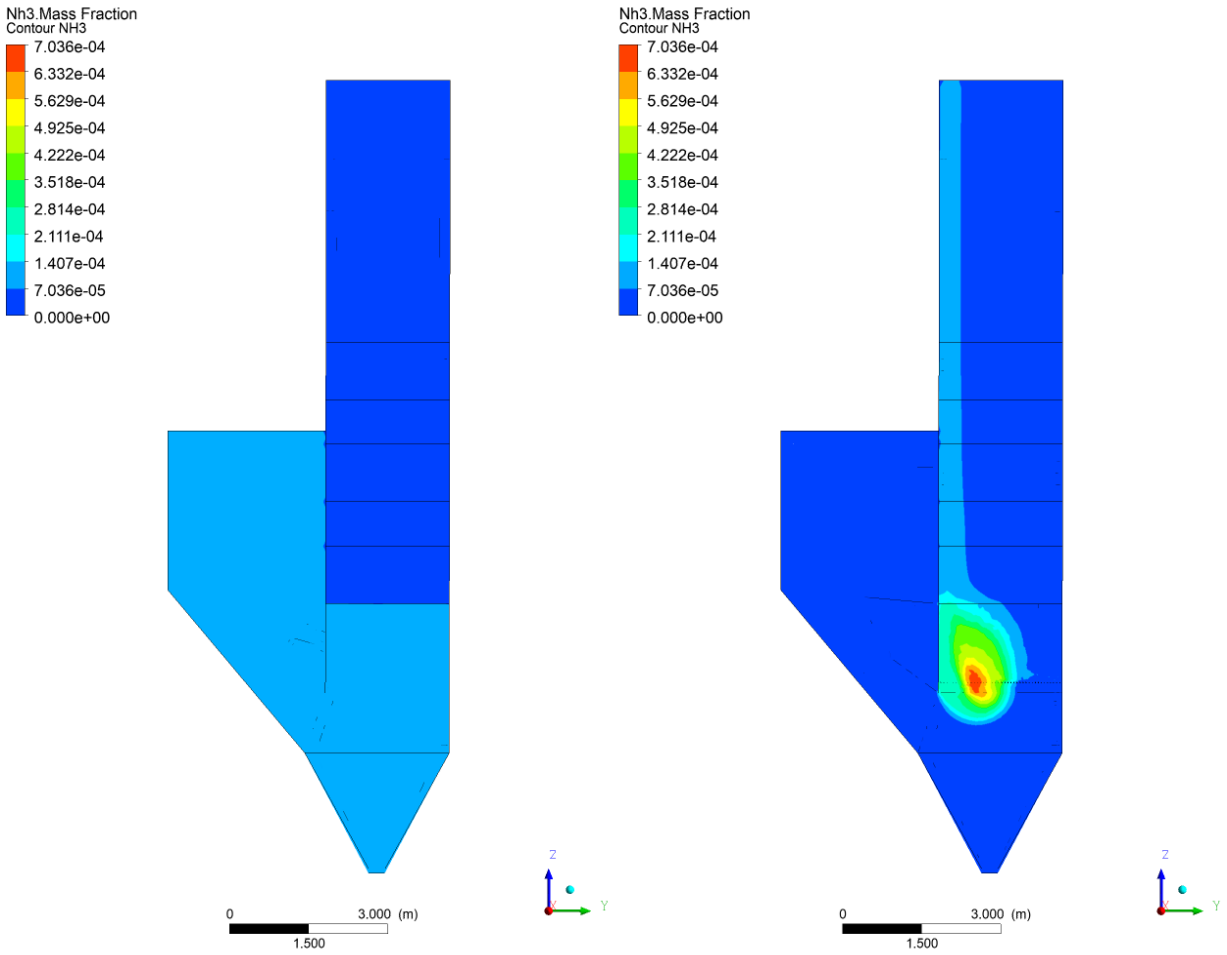

Fig. 4.13 Comparison of NH_3 concentration, vertical cross-section: Ideal – left, Real – right

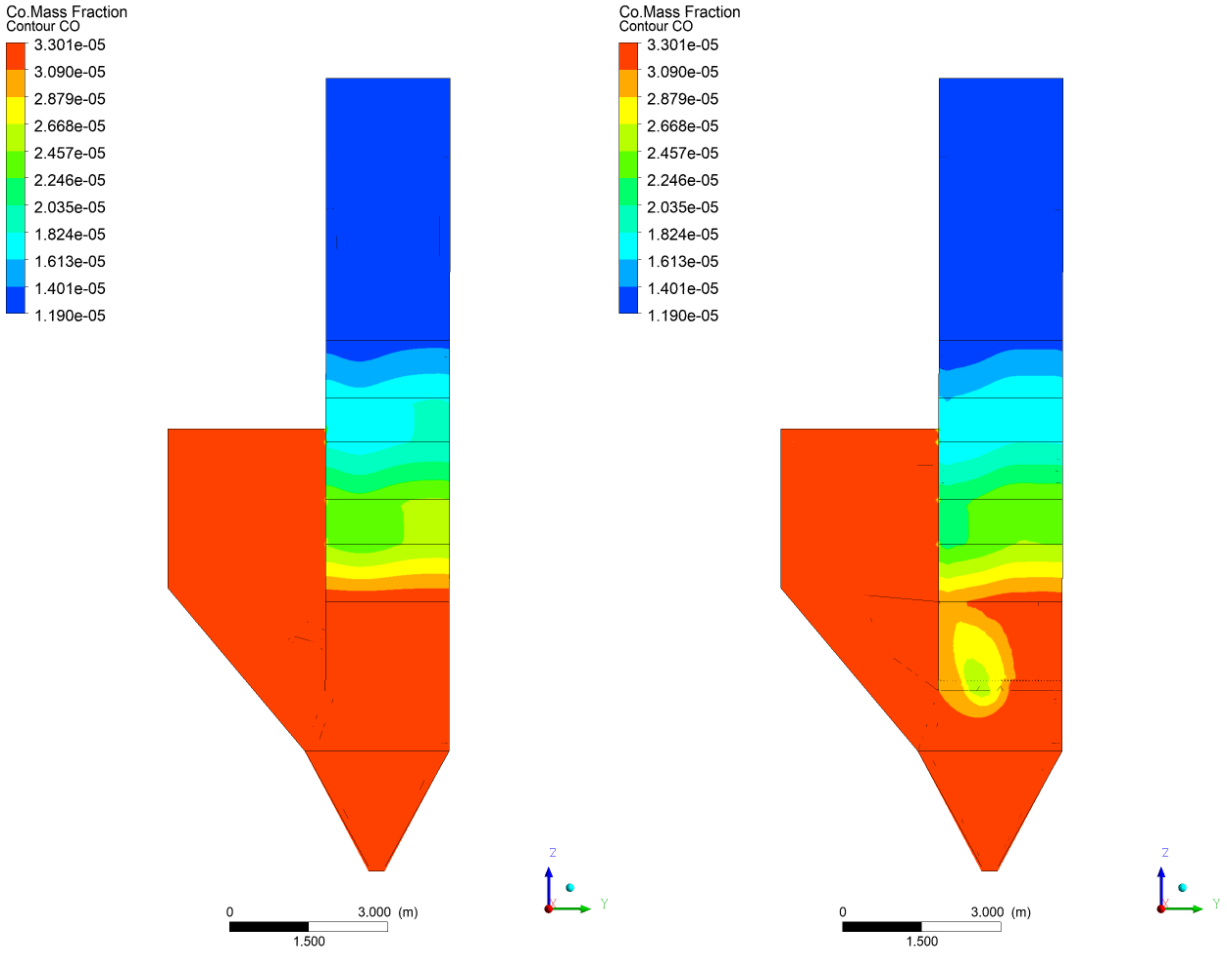

Fig. 4.14 Comparison of CO concentration, vertical cross-section: Ideal – left, Real – right

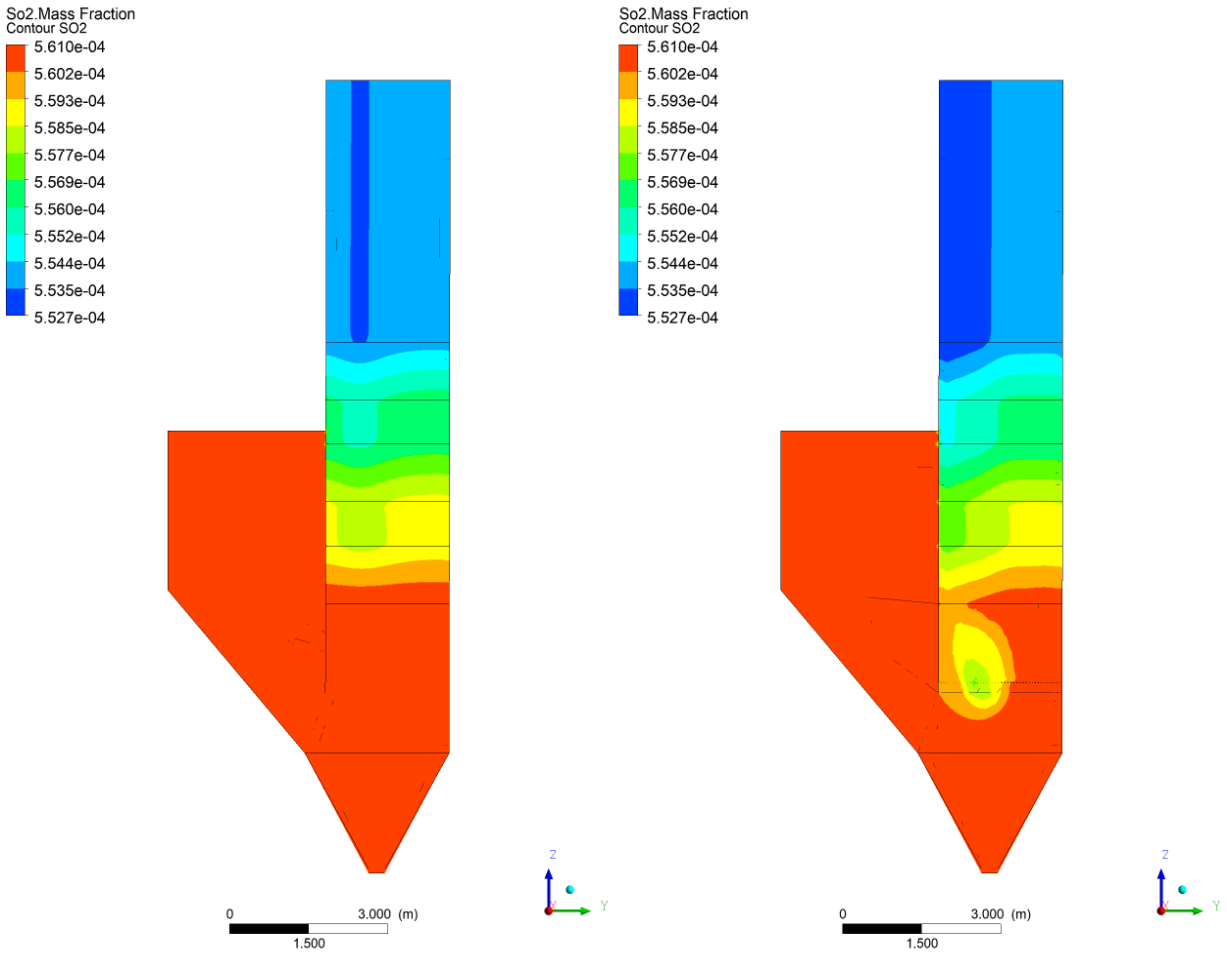

Fig. 4.15 Comparison of SO_2 concentration, vertical cross-section: Ideal – left, Real – right

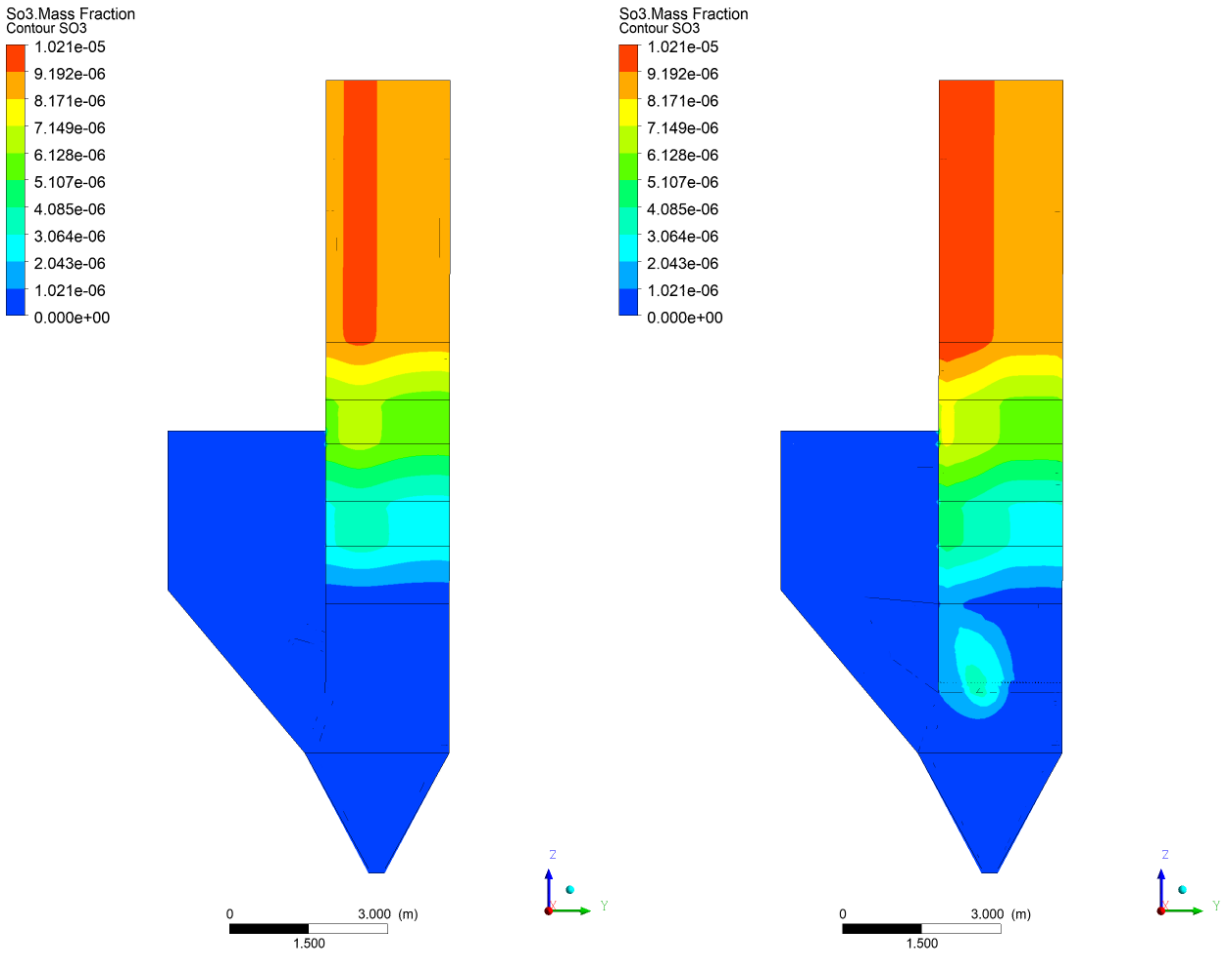

Fig. 4.16 Comparison of SO_3 concentration, vertical cross-section: Ideal – left, Real – right

5 Conclusion

The report deals with numerical simulation of the selective catalytic process (SCR) to reduce NO_X emission of power and/or heating plant or incinerator plant (energy waste). The chemical process of NO_X is relatively complicated, but three summary reactions can simplify it.

$$1\ NH_3 + 1\ NO\ +\ 0{,}25\ O_2 \rightarrow 1\ N_2 + 1{,}5\ H_2O$$

$$SO_2 + 0{,}5\ O_2 \rightarrow SO_3$$

$$CO + 0{,}5\ O_2 \rightarrow CO_2$$

These reactions can describe the SCR process relatively precise, especially the reduction of NO_X. Secondary effects of SCR like CO reduction and conversion of SO_2 to SO_3 can be described too.

SW Fluent was used to perform simulations. Open-source code can be used too, but theory and user guides are not usually available and fully explained. Thus, the commercial SW like Fluent is the best choice for complicated CFD simulation with surface reactions.

Three variants of the SCR reactor were simulated based on task data. Generally speaking, the results of the CFD simulation is consistent with the expected results specified in task data. So, we can say, the SCR process can be modelled very accurately. On the other hand, the precision of CFD simulation is strongly influenced by catalyst data, e.g., pore surface, the activity of the catalyst, and especially chemistry for the specified type of catalyst. Experimental data for TiO_2 catalyst was available in the article, so many unknown parameters were found, and they were calculated based on the research project. Exact chemistry data other types of catalysts are necessary to generally valid CFD model of SCR.

Bibliography

[1] RASOOL, S. I. *Chemistry of the Lower Athmosphere,* Springer US Plenum press, ©1973, ISBN 978-1-4684-1988-7

[2] HEIDE, Bernd von der. et al.: *NOx-Minderung an einem steinkohlebefeuerten Kessel in der ehemaligen CSFR nach dem NOxOUT-Verfahren,* VGB-Konferenz Kraftwerk und Umwelt 1993,Essen, 28. April 1993.

[3] KOHL, Arthur L. and NIELSEN Richard B. *Gas Purification, Fifth edition,* Gulf Publishing Company, Houston, Texas, ©1997, ISBN 0-88415-220-0

[4] Blair et al., 1981

[5] LYON, R.K. *Method for the Reduction of the Concentration of NO in Combustion Effluents Using Ammonia*. U.S. Patent No. 3,900,554., 1975

[6] MILLER, James A. and BOWMAN, Craig T. *Mechanism and modeling of nitrogen chemistry in combustion,* Progress in Energy and Combustion Science, Volume 15, Issue 4, 1989, Pages 287-338,

[7] ANSYS Fluent Theory Guide, ANSYS, Inc., 275 Technology Drive Canonsburg, PA 15317.

[8] CHRISTOPHER J. Cramer. *Essentials of Computational Chemistry,* John Wiley & Sons Ltd, The Atrium, Southern Gate, Chichester, West Sussex PO19 8SQ, England, September 2004, ©2004, ISBN 978-0-470-09182-1

[9] Blejchař, T.: CFD model of NO_X reduction by SNCR method, Sborník vědeckých prací VŠB-TU Ostrava, VŠB-TU Ostrava 2009, ISBN 978-80-248-2131-3,

[10] CARTON, J.A., and SIEBERS, D.L. *Comparison of Nitric Oxide Removal by Cyanuric Acid and by Ammonia,* Combustion Science and Technology, Vol. 65, pp. 277-293, Received 14 Nov 1988, Accepted 26 May 1989, Published online: 30 Mar 2007

[11] NIST chemical kinetisc diabase, available from http://kinetics.nist.gov/kinetics/index.jsp,

[12] NOx selective catalytic reduction (SCR) on self-supported V–W-doped TiO2 nanofibers

[13] Modelling of selective catalytic reduction (SCR) of Nitric Oxide with Ammonia using four modern catalysts.